Mechanistic and kinetic studies of benzyl alcohol photocatalytic oxidation by nanostructured titanium (hydro)oxides: Do we know the entire story?

Dimitrios A. Giannakoudakis [a,b,*], Abdul Qayyum [a,**], Mariusz Barczak [c], Ramón Fernando Colmenares-Quintero [d], Piotr Borowski [c], Konstantinos Triantafyllidis [b], Juan Carlos Colmenares [a,**]

[a] Institute of Physical Chemistry, Polish Academy of Sciences, Kasprzaka 44/52, 01-224 Warsaw, Poland
[b] Department of Chemistry, Aristotle University of Thessaloniki, 54124 Thessaloniki, Greece
[c] Institute of Chemical Sciences, Faculty of Chemistry, Maria Curie-Sklodowska University in Lublin, 20-031 Lublin, Poland
[d] Faculty of Engineering, Universidad Cooperativa de Colombia, Medellín 50031, Colombia

ABSTRACT

Selective upgrade of lignocellulosic biomass-derived aromatic compounds by photocatalytic oxidation is assumed as a prosperous, environmentally friendly, and cost-effective process. We present for the first time the application of various advantageous titanium oxide nano-photocatalysts for the additives-free selective partial oxidation of benzyl alcohol to benzaldehyde at ambient conditions. The two best-performing materials were found titanate nanotubes and nanocores of anatase surrounded by amorphous titanium hydroxide phase. The results obtained by scavenger tests on top of the DFT calculations led us to conclude that various reactions and active species are responsible by a complex way for materials' photoreactivity. Depending on nanocatalysts' physicochemical features as well as the light irradiation (ultraviolet vs. royal-blue), different mechanisms/oxidation-pathways are photo-catalyzed. Finally, we show that utilizing organic compounds like benzoquinone as scavenger hides risks due to the interactions with the targeted to be converted organic that results in elevated photolytic decomposition even under royal-blue light.

1. Introduction

Novel synthetic chemistry methods as for instance the mass production of high valuable platform compounds and fine chemicals from abundant and recycling raw materials, like biomass and organic wastes, is within the hot topics of scientific research with an orientation of curricular (bio)economy strategies of development towards a "green" and sustainable future [1–3]. A plethora of aromatic alcohols can be obtained from the valorization of lignocellulosic biomass [4–6], which is assumed as one of the most abundant worldwide renewable feedstocks. Aromatic aldehydes are widely used as precursor for the industrialized synthesis of various agrochemicals, pharmaceuticals, drugs, vitamins, dyestuff, fragrance or even as additives [7,8]. Hence, the efficient and selective partial oxidation of the biomass-derived aromatic alcohols to the corresponded aldehydes is ultimately important [9,10]. The traditional approaches of aromatic alcohols oxidation involve non-catalytic protocols using harmful reagents at stoichiometric ratio and elevated pressure or/and temperature of operation. Towards developing of more environmentally friendly and cost-effective approaches, the design of catalytic methods driven/activated by different sources of energy and utilizing advantageous (nano)catalyst is on its infancy, with the heterogeneous photocatalysis using nanostructured materials to be considered among the most prosperous candidates [11,12]. Nanostructured titania oxide based catalyst were presented as popular and effective candidates for various heterogeneous photo-assisted transformation of organic compounds, especially for environmental remediation applications [13–16]. In the case of the latter applications, the ultimate goal is to unselectively decompose/mineralize the organic pollutants by the uncontrollable generation of photoinduced electron and hole pairs as well as free radicals like hydroxyl radical ($OH^\bullet$), superoxide radical ($O_2^\bullet$), and hydroperoxyl radical ($HOO\bullet$) [17]. On the contrary regarding catalytic synthetic chemistry applications, the most

---

crucial aspect is to achieve elevated conversion and kinetics of reaction, keeping simultaneously the selectivity to the targeted compound as high as possible. To achieve so, the design and development of the proper photocatalyst is vital. Depending on the physicochemical features of the (nano)photocatalyst and more importantly of its photoreactivity, is possible to manipulate the nature and the formation rate of the desired reactive oxygen-containing species in order to elevate the selectivity of the photo-assisted process. Hence, the knowledge of the involved mechanisms responsible for the photoreactivity is important.

The focus of this study was to monitor the heterogeneously photocatalyzed reaction of the selective partial oxidation of a lignin-derived model compound, benzyl alcohol (BnOH) to benzaldehyde (PhCHO), in order to determine the involved mechanism and which physicochemical features of different titanium/titanate oxide nanomaterials play a key role. The reactions were taken place at ambient and controlled conditions of temperature and pressure (30 °C and 1 atm), avoiding the addition of chemical reagents/oxidants. As light sources were used low intensity light-emitting diodes (LED)s producing ultraviolet (UV, 365 nm) and royal blue (RB, 465 nm) beams of light. Various organic or inorganic compounds were used as scavengers of different reactive species in order to conclude for the involved mechanisms.

From the point of view of the studied photocatalysts, eight nanomaterials were pre-screened. The commercially available nanoparticles of TiO$_2$ P25 and P90 and their calcinated at 600 °C counterparts were used as benchmark samples. Ultrasound treated in basic solution counterpart of P25 was also tested in order to determine if and how specific physicochemical features, specifically the surface heterogeneity [18], can affect the photocatalytic reactivity. Another sample was a multiphase nanoporous titanium oxide/hydroxide synthesized by a low-power high-frequency (500 kHz) ultrasound-assisted precipitation protocol (LPHF-US) and without being further calcined [19]. This material, herein referred to as USprec, consists of nanoparticles (20–150 nm) made of anatase cores (4–7 nm in size) surrounded by an amorphous phase grafted with carbon and oxygen containing functionalities. The other two nano-samples were titanate nanotubes obtained after ultrasound assisted hydrothermal process using P25 or P90 as precursors. Having various materials with diverse physicochemical features, in addition with DFT calculations as well as photocatalytic results using organic and inorganic scavenger tests, it would be feasible to shed light on the involved mechanisms and the reactive species that are responsible for the selective photocatalytic partial oxidation of BnOH. Finally, combination of all the above with the existing literature will lead to a comprehensive analysis of the photocatalytic partial oxidation of benzyl alcohol.

2. Experimental

2.1. Materials

Benzyl alcohol (BnOH, 99.5%, ChemPure), benzaldehyde (PhCHO, ≥99.5%, ChemPure), acetonitrile (AcN, HPLC grade), Oxalic acid (OA, ≥98%, Alfa aesar), Potassium iodide (≥99.5%, ChemPure), p-benzoquinone (BQ, ≥98%, sigma Aldrich), silver nitrate (Stan lab), 2-butanol (t-B, ≥ 99% Carl Roth) were used. All chemicals were used as received without any further purification. MiliQ water was only used.

2.2. Materials synthesis and characterizations

Various nanostructured titanium oxide/hydroxide materials were used as (photo)catalysts. The first ones were the commercially available nanoparticles TiO$_2$ P25 (Evonik) and TiO$_2$ P90 (Evonik), which were used as obtained or after thermal treatment at 600 °C. Another studied material was obtained after ultrasound treatment (37 kHz) of TiO$_2$ P25 in a strongly basic aqueous solution (10 M, NaOH) for 6 h at 67 °C, referred to as P25-US with more details to be found elsewhere [18].

A low-power high-frequency (500 kHz) ultrasound-assisted precipitation synthesis (LPHF-US) was followed for the synthesis of the nanostructured titanium oxide sample, using titanium isopropoxide in isopropanol and a NaOH aqueous solution and herein referred to as USprec [19]. Titanate nanotubes were prepared in a two-steps protocol. The first step involved the ultrasonication (37 kHz) of a strongly basic TiO$_2$ P25 or TiO$_2$ P90 aqueous dispersion, which was then (second step) transferred directly afterwards in a stainless-steel autoclave and was hydrothermally treated for 12 h at 150 °C [20]. The nanotubes obtained using TiO$_2$ P25 as precursor are referred to as TiO-NTbs or TiNTbs-25. The nanotubes were synthesized using TiO$_2$ P90 as precursor following the same protocol and are referred to as TiNTbs-90. More details regarding the syntheses and the physicochemical characterizations can be found in the Supplementary Information and elsewhere [18–20].

2.3. Photocatalytic selective oxidation experiments

The photocatalytic activity of different nano-morphologies of TiO2 was studied by monitoring the additives-free partial oxidation of benzyl alcohol (BnOH) to benzaldehyde (PhCHO) in acetonitrile. For each photocatalytic experiment, 15 mg of each catalyst was suspended in 15 mL of 1 mM BnOH solution in acetonitrile solvent. The reaction was held under constant magnetic stirring (600 rpm) during the whole photocatalytic reaction. The temperature inside the reaction vial was maintained at 30 °C by immersion inside a water bath. The entire setup can be seen in Scheme 1. Dark adsorption studies were also carried out in order to ensure the sufficient interaction between the nano-catalyst and benzyl alcohol molecule and to estimate the materials' adsorption efficiency. The duration of adsorption equilibrium was established for 1 h before the light illumination.

The photocatalytic tests were carried out under the light irradiation of low-power produced by LEDs, either ultraviolet (365 nm, power =450 mW) and Royal Blue light (465 nm, power =450 mW). The samples were collected after 0, 1, 2, 3, 6 h of light radiation for each experiment. The collected samples were analyzed by Gas Chromatograph (Shimadzu GC-2010) equipped with flame ionization detector. The capillary column (ZB-5MS) with 30 m length and 0.25 mm inner diameter with 0.5 μm film thickness was used for the analysis. The chromatograms were obtained by injecting 1 μL of sample with a split ratio of 8. The column temperature was set at 50 °C for 3 min and increased to 300 °C (rate 9 °C/min) with a final holding time of 2 min.
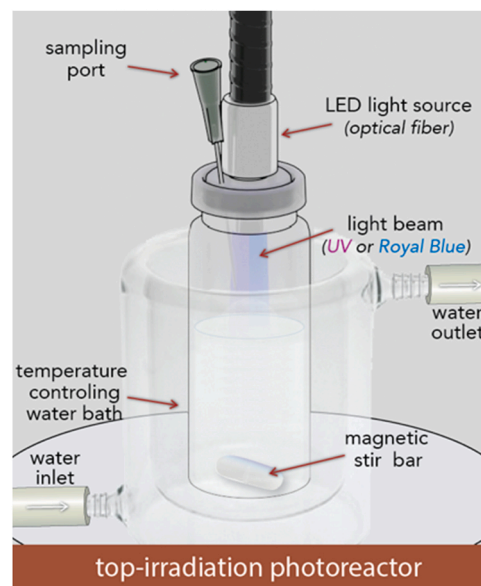
Scheme 1. Schematic illustration of the setup utilized for monitoring the photocatalytic oxidation benzyl alcohol (BnOH) to benzaldehyde (PhCHO).

Helium was used as a carrier gas. The evaluation of the photocatalytic tests was performed by monitoring benzyl alcohol (BnOH) conversion, selectivity and yield for benzaldehyde (PhCHO) as the product of the partial oxidation of BnOH. The used equations are presented in the Supplementary Information. Photolysis tests either under ultraviolent or royal blue irradiation showed that both BnOH and PhCHO are stable even after 24 h of irradiation.

2.4. Reactive oxygen species monitoring (Scavenger tests)

A series of control experiments were carried out by the addition of various compounds, organic or inorganic, known acting and utilized as active species scavengers in order to identify the main reactive oxygen species (ROSs) that can be responsible for BnOH or/and PhCHO conversion. The concentration of the scavenger substance per initial concentration of BnOH was equimolar (1:1). Oxalic acid (OA) and potassium iodide (KI) were used as h^+ scavenger [21], silver nitrate (Ag) as e^- scavenger [22], 1,4-Benzoquinone (BQ) as $O_2^{\bullet-}$ scavenger [23], and tert-butanol (t-B) as $\bullet$OH scavenger [21].

2.5. DFT computational studies

The interaction of benzyl alcohol, benzaldehyde, acetonitrile, water as well of all the utilized organic compounds as scavengers with different surface functional groups potentially available on the materials' surface (Figure S1) were investigated based on density functional theory (DFT) calculations (B3LYP). Additionally, the intermolecular energy of interaction between the organic utilized moieties were also determined. More details can be found at the Supplementary Information.

3. Results and discussion

3.1. Photo-oxidation under UV and RB light (preliminary screening)

In the first series of screening experiments, the photocatalytic efficiency of eight titanium oxide based semiconductor nanomaterials was evaluated under low power royal blue light (RB, 465 nm) irradiation from LED (Fig. 1a). The targeted reaction was the selective oxidation of benzyl alcohol (BnOH) to benzaldehyde (PhCHO) under ambient conditions and without the addition of reagents/oxidizing agent. Since the band gap of the herein studied materials (3.2 ± 0.2 eV) is in the range of ultraviolet A (UVA), no photoreactivity would be expected theoretically under royal blue light exposure, considering in addition that the materials did not reveal any light absorption at the visible range (except the nanotubes that exhibited visible light absorption to a small extend) as can be seen in Figure S2. Although, it is well-known that specific TiO_2 materials, as for instance the commercial TiO_2 P25 or anatase TiO_2, have photocatalytic activity even under visible light exposure [24–28]. This effect can be predominantly linked to different phenomena. The first one is the photosensitization mechanism, known also as "antenna" light scavenger effect, which is attributed to the formation of surface complexes between the organic compounds and specific surface functional groups [28–30]. It was showed that the presence in particular of surface hydroxyl groups in titanium dioxide particles is crucial since these groups can be involved in the adsorption of alcohols and the formation of surface complexes [31] leading to the photosensitization effect and hence to photoactivity under visible light irradiation [27,28]. DFT calculations showed that the adsorption of BnOH on surface hydroxyl groups may result in the formation of intermediate alkoxide moieties and due to hybridization electron transition from the complex to the conduction band takes place under visible light exposure [32]. The visible light-induced selective oxidation of various aromatic and aliphatic alcohols by dye-sensitized anatase TiO_2 was also presented previously [24]. Another reason for the visible light photoreactivity can be linked to the presence of surface defects which can also induce
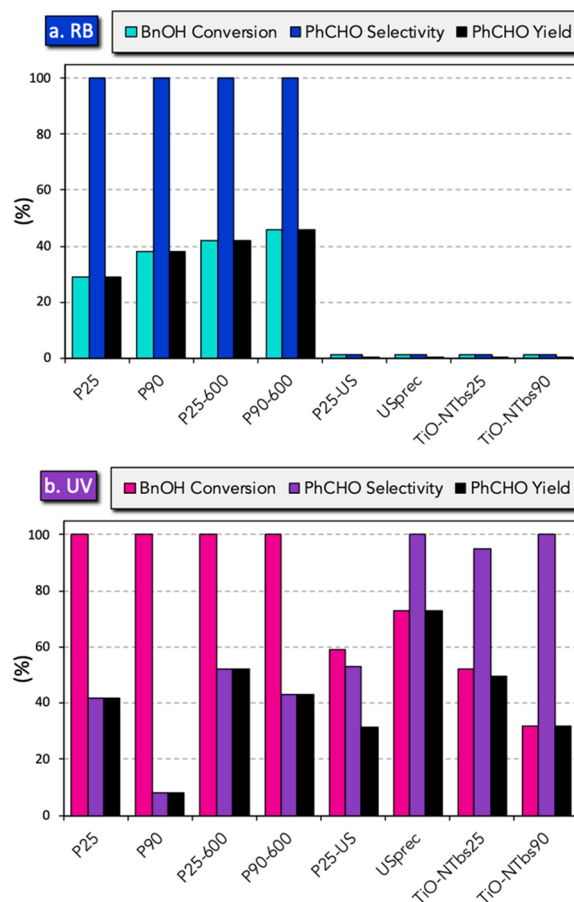

Fig. 1. Conversion of BnOH (1 mM), PhCHO selectivity and yield after 6 h of exposure of low power ultraviolet (UV, 365 nm) (a) and royal blue (RB, 465 nm) (b) at 30 °C (600 rpm stirring) and using 1 g/L of the photocatalyst in 15 mL of an initial 1 mM BnOH solution and acetonitrile as solvent.

photoreactivity under visible light since the required energy for local electron excitation is lower as for instance was presented for black titania samples [33,34]. Thus, the possible interactions of benzyl alcohol with different surface functional groups that can be found on titanium oxide materials were further studied in this work by DFT calculations as well as by comparing different titanium oxide nanocatalyst with different surface properties.

After 6 h of irradiation, TiO_2 P25 showed a 27% BnOH conversion with a 100% PhCHO selectivity. Calcination of P25 at 600 °C (P25–600) had a positive impact, since the BnOH conversion reached 40.5% with the selectivity to be retained 100%. P90 showed a higher conversion (39%) than that of P25, while calcination at the same temperature (P90–600) had a minimal positive effect with the yield reaching 44%. Both P90 and P900–600 showed a 100% PhCHO selectivity. The two found differences between the as received and their calcinated at 600 °C counterparts are regarding the crystallinity (size of each crystal phase and ratio of anatase:rutile) and the water content. Based on XRD analysis (Figure S3), calcination led to a decrement of the anatase content from 86% to 81% for P25 and from 92% to 85% for P90. On the contrary, the crystalline sizes of the anatase phase for P25 increased from 17.5 to 19.0 nm, while the rutile phase from 23.7 to 28.4 nm. For P90, the crystalline size of anatase increased from 10.8 to 13.6 nm and of rutile from 15.5 to 21.8 nm. Thermal treatment of the materials (150 °C in air for 2 h) revealed weight losses of 1.1%, 0.4%, 1.9%, and 0.5% for P25, P25–600, P90, and P90–600, respectively, assigned mainly to the removal of the adsorbed atmospheric humidity. It should be pointed out that the alterations in photoactivity between the calcinated and the as received (pristine) samples can be also linked to the presence of an

amorphous phase for the pristine commercial nanomaterials [35], since it was expected that calcination above 500 °C would lead to the crystallization of the amorphous phase. Additionally, the enhancement of the photocatalytic efficiency can be linked to the increase in ratio of anatase to rutile, as well as to the increase of the crystals' size [36,37]. Another possible reason is that more catalytic sites become available by the removal of hydrogen-bonded water molecules.

Regarding the home-made materials were not found capable to initiate the conversion/oxidation of BnOH under low power RB light exposure. It is interesting that the sample obtained after ultrasound treatment of commercial TiO$_2$ P25 in a strongly basic solution (P25-US) in order to enhance the surface functionality and reactivity [18], did not reveal any photoreactivity under RB light exposure, as well the other three lab-made samples. In the case of P25-US, we link this to the neutralization of the Lewis acidic catalytic sites during the ultrasound-assisted treatment with strong base and to the reported formation of an external layer around the nanoparticles [18]. Even though this layer has an amorphous nature, and it is reach in hydroxyl surface functional groups, P25-US was found totally inactive under RB light exposure. This layer acts as a "surface shield" towards favorable adsorption of BnOH, blocking the photosensitization/antenna effect and/or the formation of surface complexes of high stabilization energy (as we will present and discuss herein afterwards). Another reason can be that the synthetic protocol leads to de-aggregation during ultrasonication, and so different aggregation patterns occurs during filtration and drying after the hydrothermal treatment. In general, the photoreactivity can be affected by various parameters as discussed above, such as crystallinity (nature, degree, and size), surface chemistry, and presence of moisture, with all these parameters to antagonistically affect the BnOH conversion and PhCHO selectivity [37].

In the case of low power ultraviolet irradiation (UV, 365 nm), all the materials presented elevated BnOH conversion. For P25, the BnOH conversion reached 100% after 6 h, with a PhCHO selectivity of 41%, and hence equal yield. No benzoic acid or other aromatic compound were detected, suggesting that BnOH undergo photodecomposition either via the formation of aromatic aldehyde (which further and unselectively decomposed/mineralized) or via other pathways. P90 also showed an absolute conversion, although the selectivity was as low as 7%, suggesting a more intensive ability to faster decompose PhCHO. Calcination of the commercial samples had a positive effect on the selectivity, since for P25–600 and P900–600 were 53% and 41%, respectively. Ultrasound treatment of P25 in a basic solution (P25-US) led to a decrement of the conversion efficiency by 40% comparing to pristine P25, but on the contrary the selectivity was increased by ~50% and hence the PhCHO yield was 31%.

The material obtained by ultrasound-assisted precipitation (USprec) showed an absolute selectivity to PhCHO, while the BnOH conversion was 76%, leading to the highest yield (76%) between all the herein studied materials. The titanate nanotubes obtained from P25 as precursor (TiNTbs-25) [20], showed 53% of conversion and 88% selectivity, leading to a 47% yield. The titanate nanotubes obtained with the same synthetic protocol as TiNTbs-25 but using TiO$_2$ P90 as precursor (TiNTbs-90) showed significantly lower value for conversion (37%) and yield comparing to TiNTbs-25.

These results guide us to explore further the photocatalytic selective oxidation bearing in mind the possibility that different reactions, mechanisms and surface interactions are involved, while the irradiation with RB comparing to UV irradiation leads to the formation of different active species. Additionally, we would like also to explore the option that especially upon UV irradiation, more than one oxidation pathways are occurring simultaneously but with a different rate and at different catalytic sites. Towards the exploration of the abovementioned directions and to extract easier the main messages and conclusions, the focus was concentrated on three materials with unique physicochemical features and more importantly totally different morphology and surface chemistry; the commercial benchmark catalyst (P25) and two home-made materials, the one obtained from ultrasound-assisted precipitation (USprec) and the titanate nanotubes using P25 as precursor (TiO-NTbs). It is the first time to the best of our knowledge that this kind of novel nanomaterials are tested in detail for the selective partial photocatalytic oxidation of the cellulosic biomass derived model compounds, benzyl alcohol.

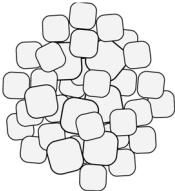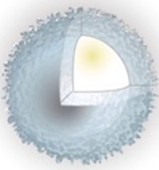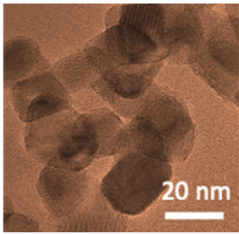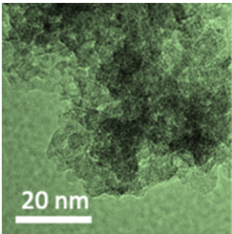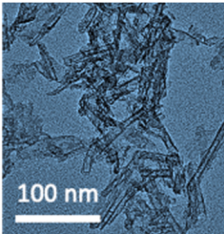### 3.2. Physicochemical features of the photocatalysts

The most important physicochemical features and parameters of the three photocatalysts are collected in Table 1, while the N$_2$ sorption isotherms as well as the pore size distributions, powder XRD patterns, thermal gravimetry profiles, and potentiometric titration analysis in Fig. 2, while ATR-FTIR spectra (Figure S4) and low magnification TEM images (Figure S5) are presented in Supplementary Information. The commercially available TiO$_2$ P25 is a widely studied photoreactive nanomaterial that consist of TiO$_2$ nanoparticles of two different crystallinities, anatase and rutile, with the former to be the predominant one (83%) [18]. The average crystalline size for anatase was found as 17.5 nm, while of rutile as 23.7 nm. An amorphous phase also exists, although not feasible to be determined by XRD [35,38]. The band gap of the semiconductor P25, estimated based on diffuse reflectance approach and the derived Tauc plots, was 3.2 eV, while the specific surface area (S$_{BET}$) and the total pore volume (V$_{Tot}$) were found 55 m^2/g and 0.192 cm^3/g, respectively [18]. For USprec, the structure was described as aggregates of spherical-like nanoparticles (20–150 nm) consisting of anatase nanocrystals (4–7 nm in size) as cores surrounded by an amorphous and nanoporous titanium (hydro)oxide phase reach in hydroxyl groups as well as in carbon and oxygen containing functionalities [19]. The band gap of USprec was estimated as 0.1 eV higher than that of P25. The textural features were found significant higher in values compared to P25, since the S$_{BET}$ was 326 m^2/g and the V$_{Tot}$ 0.484 cm^3/g [19]. In the case of the hydrothermally synthesized nanotubes (TiO-NTbs), it was found that they are built from titanate (H$_2$Ti$_3$O$_7$) nanosheets scrolled to open-ended tube-like nanostructures, with external and internal (empty space/channel size) diameter of 17 ± 5 and 4–11 nm, respectively, while the length of the nanotubes was in the range from 50 to 150 nm [20]. The high S$_{BET}$ (300 m^2/g) is slightly lower comparing to USprec, but on the contrary the V$_{Tot}$ almost by two folds higher, reaching 0.873 cm^3/g, a value notably high for metal oxide based material [20].

Since we showed previously that the presence of water has a negative impact on the benzyl alcohol photo-oxidation performance for P25 [39], the amount of the pre-adsorbed humidity, physically or chemically, as well as of the structural water was estimated by thermal analysis under He atmosphere (Fig. 2d-e). As can be seen from the weight losses in Table 1, P25 showed the least weight loss, followed by USprec and then by TiO-NTbs. The latter sample was expected to have the highest amount of water due to its structure, since water molecules are intercalated between the titanate layers with the general chemical formula of this material found as H$_2$Ti$_3$O$_7$•1.9 H$_2$O [20], while water molecules can be strongly retained withing the nanorod structure. For USprec, the also elevated amount of moisture is due to the porous nature of the phase surrounding the anatase cores [19].

The surface functional groups (SFGs) were calculated by potentiometric titration (PT) analysis and the results for the SFGs with pK$_a$< 7 and pK$_a$> 7 are collected in Fig. 2f-g [18–20]. The former ones are linked to the bridging and acidic terminal oxygen containing groups, while the later to the basic terminal hydroxyl groups [18–20]. It can be observed that the synthesized materials have enormously higher amount of SFGs comparing to P25 especially above pK$_a$ of seven. Ti-NTbs have both the highest amount above and below pK$_a$ of seven. Based on the deconvolution of O 1 s core energy-level spectra of XPS analysis presented and analyzed elsewhere [18–20], the predominant oxygen functional groups (94.4%) for nanotubes were assigned to the bridging Ti-O-Ti of the H$_2$Ti$_3$O$_7$•1.9 H$_2$O structure, while the rest to hydroxyl groups at the tubes' edges [20]. For USprec sample, no Ti-O-Ti

Table 1

The main physicochemical features of the herein studied photocatalysts as previously reported [18–20].

	TiO$_2$ P25	USprec	TiO-NTbs
Synthesis	As received[18]	Ultrasound assisted precipitation of TTIP in basic solution[19]	Hydrothermal treatment of P25-US[20]
Key features	A well-know and widely studied commercial nano-photocatalyst, used as benchmark photocatalyst.	A combination of anatase nanocrystals as cores surrounded with amorphous phase with high density of hydroxyl surface groups.	Titanate nanosheets (H$_2$Ti$_3$O$_7$ *1.9 H$_2$O) scrolled in open-ended nanotubes with interlayer spacing between the titanate layers of 0.92 nm.
Potential catalytic sites	External surface of the nanoparticles.	Pores of the outer amorphous phases and the core's surface.	External surface and free space inside the tube structure.
Structure			
TEM			
Avg. size of particles	5–45 nm	Central anatase cores: 4–7 nm Total size of the spherical-like nanoparticles: 20–150 nm	external diameter of 17 ± 5 nm, an internal diameter of an empty space (channel size) of 4–11 nm and lengths from 50 to 150 nm
Detected crystal phases in % *	Anatase (83%): Rutile (17%)	Anatase (100%)	Tubular shaped layers of Ti$_3$O$_7^{2-}$
Avg. crystals sizes (nm) *	Anatase: 18 / rutile: 25	4	–
S$_{BET}$ (m^2/g)	55	326	300
V$_{Tot}$ (cm^3/g)	0.192	0.484	0.873
V$_{mic}$ / V$_{2-10}$ / V$_{>10}$ (cm^3/g)* *	0.005 / 0.018 / 0.043	0.031 / 0.209 / 0.041	0.021 / 0.222 / 0.503
Band gap (eV)	3.20	3.30	3.24
Weight loss up to 140 °C (%)* **	1.0	4.4	6.8
Weight loss up to 390 °C (%)* **	1.7	8.0	10.0
Weight loss up to 600 °C (%)* **	1.9	8.7	10.4
Surface pH	5.1	4.0	7.1
Surface Functional groups (SFGs) pKa< 7 / pKa> 7 (mmol/g)* ** *	0.07 / 0.05	0.4 / 1.48	0.59 / 2.13
Surface Functional Groups density per S$_{BET}$ (μmol/m^2)	2.18	5.77	9.10

*based on XRD, ** based on DFT, *** based on thermal analysis in helium atmosphere, **** calculated from potentiometric titration experiments.

functionalities were detected, since the Ti-O-H acidic and basic groups were found as the main ones with an almost equal ratio and so hydroxyl groups rather oxide groups serves as the bridging moieties at the outer amorphous phase, considering that XPS analysis is a surface technique [19]. Another outcome derived from the PT analysis is that the density of the SFGs with pKa< 7 ($d_{SFGs/SA}^{<7}$) is almost the same for the three samples. On the contrary, the density of the groups of pK$_a$> 7 is dramatically higher for the synthesized samples. The differences of the surface chemistry heterogeneity influence the surface pH that was 5.1, 4.0, and 7.4 for P25, US-prec and Ti-NTbs, respectively. Considering that the ratio of the SFGs with pK$_a$> 7 to pK$_a$< 7 is around 3.6 for the synthesized samples, but the surface pH is acidic for US-prec while slightly basic for Ti-NTbs, it can be concluded that the SFGs of USprec with pKa< 7 are of a stronger nature.

The surface oxygen functional groups were analyzed also based on

the O *1 s* core energy level spectra (Fig. 3) derived by X-ray photoelectron spectroscopy (XPS). For TiO$_2$ P25 nanoparticles, the deconvolution revealed three contributions with the maxima to be allocated on 529.9, 531.2, and 532.1 eV [18]. The first contribution is linked to the lattice oxygen (Ti–O–Ti) and was representing around 84% of the total oxygen amount. The second and third ones are linked to the acidic bridging hydroxyl groups (Ti–OH–Ti) and the basic terminal hydroxyl groups (Ti–OH), respectively, with their contribution to be 10% and 6%. For TiO-NTbs, only two contributions were observed. The predominant one with a maximum at 530.3 eV (~94%) was assigned to lattice oxygens. The second with a maximum at 531.7 eV (~6%) was linked to the basic terminal hydroxyl groups (Ti–OH) (as defects at the edges of the tubes) [20]. In the case of USprec, the deconvolution revealed three contributions, with the interesting aspect to be the absence of the lattice Ti–O–Ti oxygen moieties. This can be linked to the nature of the XPS
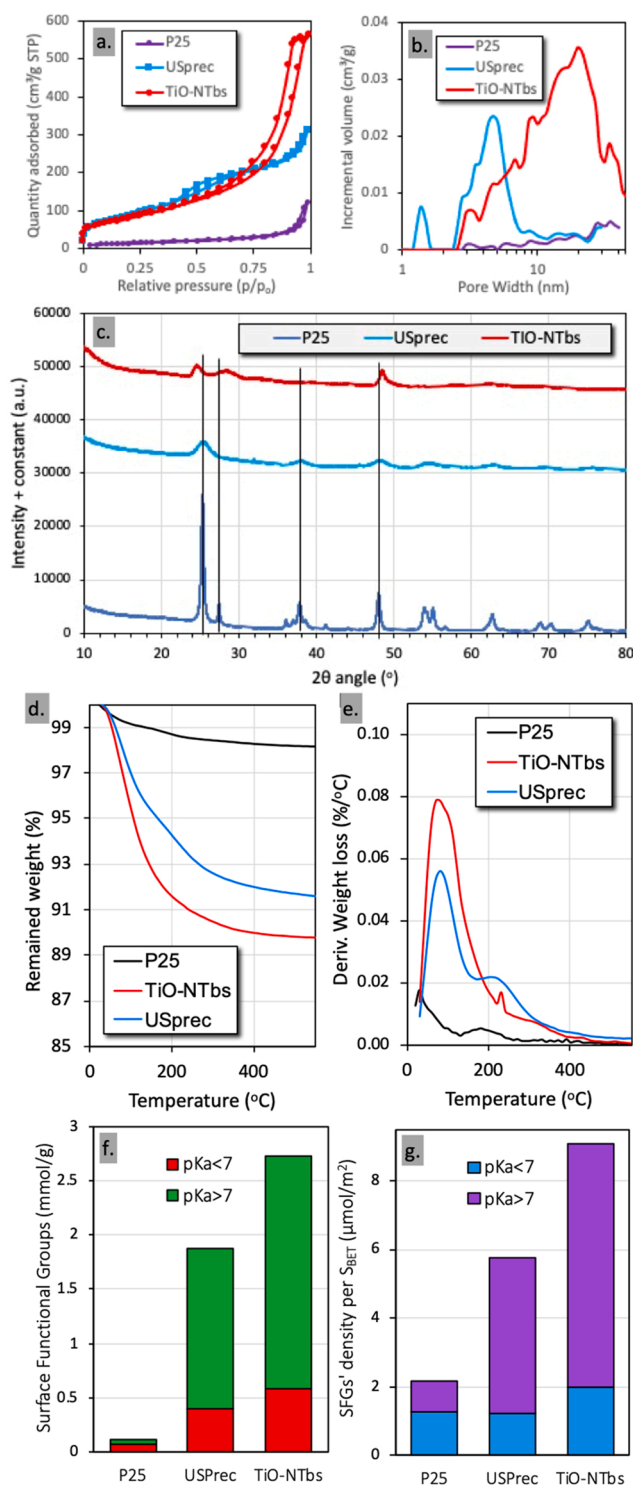
Fig. 2. N$_2$ adsorption/desorption isotherms (a), pore size distribution based on BJH model (b), powder XRD patterns (c), thermogravimetric analysis (TGA) (d) and differential thermogravimetry (DTG) (e) profiles/curves (measured up to 550 °C in helium atmosphere), the amounts of surface functional groups (SFGs) with pK$_a$ below and above 7 (f), and the density of SFGs with pK$_a$< 7 or pK$_a$> 7 per specific surface area (S$_{BET}$) as calculated based on potentiometric titration analysis (g) for TiO$_2$ P25, USPrec, and TiO-NTbs [18–20].

analysis, which as a surface technique can analyze in the range of 5–7 nm of the external surface of the nanoparticles. This outcome is aligned with the structure of the USprec nanoparticles, since the internal anatase core is surrounded with an amorphous phase grafted with
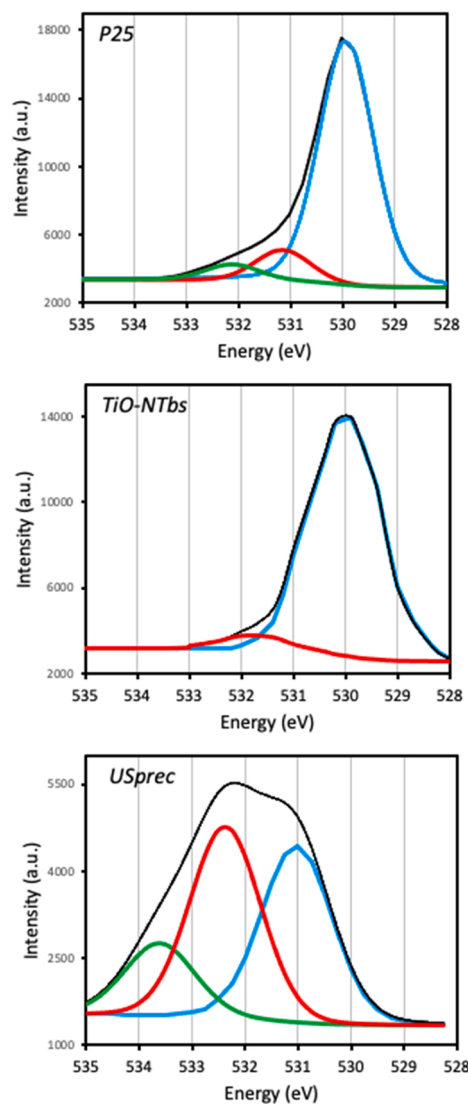

Fig. 3. Deconvoluted high-resolution core energy level XPS spectra for O 1 s [19,20].

carbon and oxygen containing functionalities [20]. The three oxygen functionalities were linked to the acidic bridging hydroxyl groups with maxima at 531.0 eV (Ti–OH–Ti), basic terminal hydroxyl groups (Ti–OH, maxima at 532.2 eV), and carbon containing functionalities linked to titanium atoms via an oxygen (Ti–O–C, maxima at 533.8 eV) [20], with their ratios to be 40%, 43%, and 17%, respectively. The XPS results support hence the higher density of the surface hydroxyl groups for the home-made materials as revealed by the thermal analysis and potentiometric titration results. We would also like to point out that in the case of potentiometric titration analysis, the materials are dispersed in water, while in the case of XPS, the material are dried at high temperature in vacuum, hence the differences, even insignificant, can be assigned to the presence or not of (adsorbed) water molecules. The materials in the thermal analysis as well as in the case of the photocatalytic tests were not pre-treated. The as prepared powders were analyzed also by ATR-FTIR, and as can be seen in Figure S4, the intensity of the bands linked to the vibration of the hydroxyl groups are of a higher intensity for the synthesized samples.

3.3. Oxidation mechanism and reactive oxygen species (ROSs)

The photocatalytic oxidation of BnOH can potential undergo through

different reaction pathways, in which different mechanisms and reactive oxygen species (ROSs) can be involved. Generally, the major ROSs responsible for advanced oxidation processes (AOPs) are the photoinduced/photoexcited electrons (e^-) and holes (h^+), hydroxyl radicals ($\bullet OH$), and superoxide anion radicals ($O_2^{\bullet -}$), which can lead to the formation of H_2O_2 and hydroperoxyl/hydrogen superoxide radical ($\bullet OOH$) [23]. The main reactions/half-reactions for the formation of all reactive oxygen-containing species (ROSs) are collected in the as we referred to it as "angel wings" photocatalytic cycle (Fig. 4) [23].

A key aspect is that various of the presented reactions can take place at the semiconductor surface simultaneously while some of them can be competitors. For instance, the formed e^- can be participate in eight different reactions as can be observed in Fig. 4 (green arrows) and which one occurs in a greater extent depend on various factors. Another important aspect is which of these reactions can be activated by the nano-photocatalyst. In order to conclude whether all these reactions can be photo-initiated by the studied materials, the valence band (VB) and conduction band (CB) energy levels for the studied samples (Fig. 5a) were estimated based on the XPS measurements (Figure S6) and the calculated band gaps. The redox potentials for the formation of all the possible ROSs are collected in Fig. 5b. It can be observed that all three samples can photo-initiate all the reactions. Interestingly, the homemade materials have VB energy level close to the redox potentials of the formation of hydroxyl radicals. This can suggest that the formation of free hydroxyl radical is not favorable and hence the better selectivity as well as the lower rate of photocatalytic conversion of organic compounds can be linked with this effect. We must trigger the attention that the values of the redox potential are sensitive to the pH in the case of aqueous solutions and even more importantly, to the solvent used.

The photoreactivity of the titanium dioxide arises from the photon absorption which leads to the photoexcitation of electron/hole pairs and as a result to the formation of various active species/radicals [42]. There are various reported mechanisms for BnOH partial oxidation which involve the photo-induced holes via a multi-steps mechanism, with the most accepted ones to presented in Fig. 6. In most of the cases, the oxidation requires a prior adsorption of the benzyl alcohol molecules on the surface, predominately by hydrogen bonds or/and charge interaction via the phenyl ring with the polar in nature surface of titanium dioxide, and the formation of surface complexes [28–30]. Hence, the presence of surface hydroxyl groups plays a pivotal role for the adsorption as well as for the formation of the surface complex [31], with both to promote light absorption (antenna light scavenger effect) and as result the photocatalytic activation/initiation [27].

In general, the "catalytic comfort zones/phases" in which the photocatalytic reactions happen should be considered to be consisting of two layers [30,39]. In the first one, referred to as stable phase, molecules of the solvent, humidity, and benzyl alcohol, as well as molecular
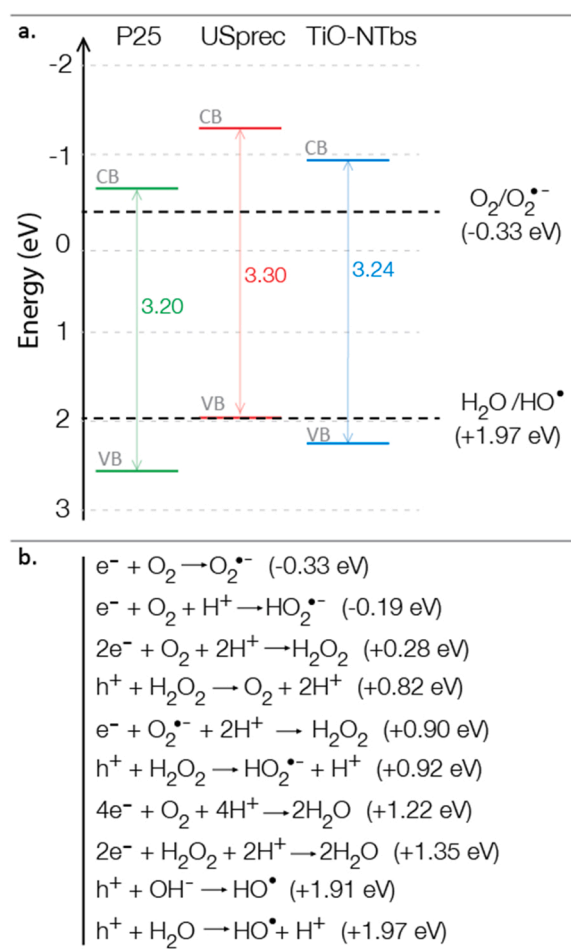

Fig. 5. (a) Schematic representation of the valence band (VB) and conduction band (CB) energy levels for the studied samples (vs. Normal Hydrogen Electrode, NHE) and (b) the redox potentials for the formation of various ROSs and reactions with emphasis on the formation of superoxide anion/radical, and hydroxyl radicals (the values of the redox potentials at pH = 7 are from the literature [40,41].

oxygen are adsorbed on the surface. In the second layer, the interface between the stable phase and the bulky phase of the dispersion, referred to as relatively mobile phase, the present molecules do not interact directly with the surface but with the adsorbed molecules of the stable phase. The photoinduced active species can react with molecules both in the stable or/and relatively mobile interphase (although the latter case is not favorable due to the shoer lifetime of the radicals). Hence, multistep BnOH oxidation can be occurred also in the relatively mobile interphase. The formed reactive species, like hydroxyl radicals, can subtract a hydrogen (deprotonation) from BnOH either from -OH or -CH_2- groups, leading to the formation of an intermediate radical, namely benzyloxy (Ph-CH_2O^*) (Fig. 6a). Zhao and co-workers showed previously that the abstraction of a hydrogen is energetically preferable to occur from the -CH_2- (stable secondary carbocation) rather than the -OH and to be initiated by a hole [23]. Further attack by a OH radical can lead to the formation of a transient diol which can be turnover to aldehyde by dehydration. Following the work of Palmisano and co-workers in which the autocatalytic photoxidation of 2-methoxybenzyl alcohol in water was supported [43], Mokari and co-workers [44], showed that the formed benzaldehyde can be transformed to benzoyl radical (Ph-$CO^\bullet$) and by reacting to BnOH to form benzyloxy radical (Fig. 6a,ii). In addition, they proposed that benzyloxy radical (PhCH$^\bullet$OH) can react with molecular oxygen leading to the formation of a PhCH(OH)$O_2^\bullet$ radical which is transformed finally to PhCHO. We have
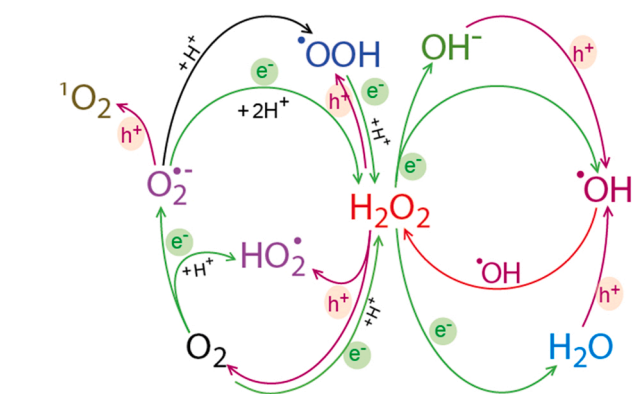

Fig. 4. The "angel wings" photocatalytic cycles of the formation of all reactive oxygen-containing species (ROSs); the reactions/half-reactions can be seen in Supplementary Information.
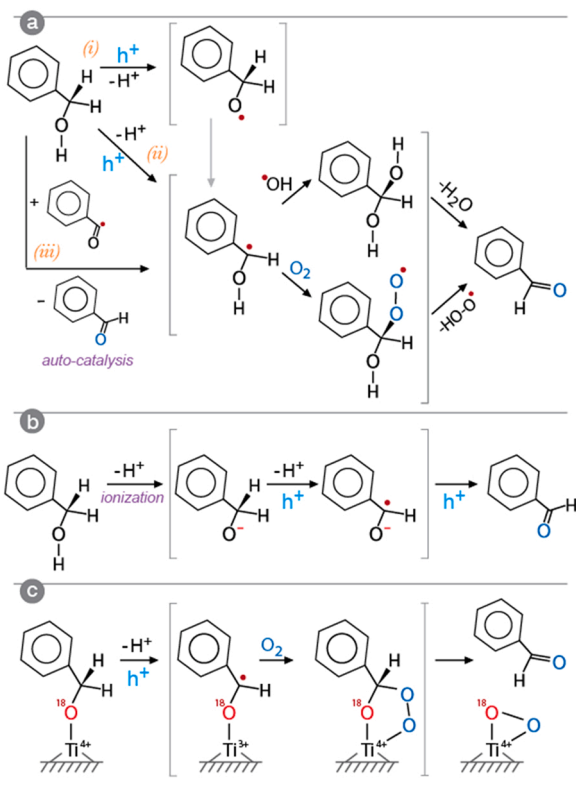
Fig. 6. The predominant photocatalytic pathways for the selective oxidation of benzyl alcohol.

to point out that the autocatalysis can be competitive to the other oxidation pathways as well to take place simultaneously but with a lower rate.

Oxidation of BnOH can also be achieved through the formation of the alkoxide anion (ionization by deprotonation), with the formed anion to be afterwards transformed with the involvement of a hole to a transient anionic radical by further deprotonation and the release of an electron (Fig. 6b). At the final step, further dehydrogenated occurs by the reaction with another photogenerated hole at the valence band and benzaldehyde is finally obtained by an intermolecular rearrangement [42, 45]. The photogenerated and released electrons can react with dissolved oxygen molecules to form $^\bullet O_2$, and hence the presence of dissolved O_2 is of a great importance as electron acceptor assisting the e^-/h^+ separation and deprotonation [28,46]. For instance, in various reports purging with inert gas led to a diminishing of the oxidation [39,46]. The water moieties, formed by side reactions or being initially pre-adsorbed on the surface of the catalyst due to humidity, have an important role since they are transformed to hydroxyl radicals by the reaction with photogenerated e^-/h^+ pairs [28,47]. These species can be also responsible for the overoxidation reactions leading either to carboxylic acids or to unselective decomposition/mineralization of BnOH or the formed oxidation products. On the contrary, the •OH can act as consuming agents of the released protons [45], helping at the deprotonation steps.

The aforementioned mechanisms require the organic molecule to be in the catalyst's interfacial zone (stable or mobile phase) in order holes to act. The formation of the radical as well as of the anion intermediates in mechanisms a and b in Fig. 5 can take place also after adsorption on the catalyst surface and formation of a surface complex. Kobayashi and Higashimoto suggested based on DFT calculations that the surface hydroxyl groups on titanate contribute pivotally to the formation of the intermediate alkoxide moieties via strong hybridization with the alcohol [32]. They also attributed the photoactivity under visible light "to the electronic transition from the donor levels created by the alkoxide

species to the conduction band" [32].

Lang et al. uncovered that the formation of "Ti side-on peroxide" occurs with a direct involvement of dissolved O_2 (Fig. 6c). Upon the formation of a complex between the TiO_2 surface and benzyl alcohol via the oxygen of the alcohol as the bridging element, deprotonation and electron subtraction by a hole takes place, leading to an intermediate radical complex formation. Molecular oxygen creates the "Ti side-on peroxide" and by two bonds heterolytic cleavages, the corresponding aldehyde is obtained among with H_2O_2. By ^{18}O isotope labeling of benzyl alcohol, they elucidated that the oxygen of the final aldehyde origins from the molecular oxygen rather than the initial one of the alcohol.

3.4. Surface interactions (DFT computational studies)

Considering all the above described selective oxidation mechanism, it can be assumed that more than one pathway can be take place solely or in parallel and with a kinetically competitive nature. Additionally, the surface chemistry of the photocatalyst and as a result how BnOH get adsorbed on the catalyst's surface is a key point needed to be explored and considered. Subsequently, we studied by DFT calculation the interactions of BnOH, PhCHO, water and acetonitrile with three different in chemical nature titanium oxide/hydroxide surface functionalities. The main goals were to determine the stabilization energies of adsorption as well as the orientation of the adsorbed molecules. For the first case of surface chemistry, all the oxygen moieties were in the form of bridging Ti-O-Ti (tit). For the second case, a hydroxyl group was bonded on Ti (tit-OH), while for the third one, a hydrogen was bonded to the bridging oxygen (tit-H).

Regarding the stabilization energies (Fig. 7), it can be seen that upon hydrogen/hydroxyl addition, all the molecules have an increased stabilization energy (ΔE_{Stab}) comparing to tit functionality, meaning a stronger interaction due to their polar nature. The highest stabilization
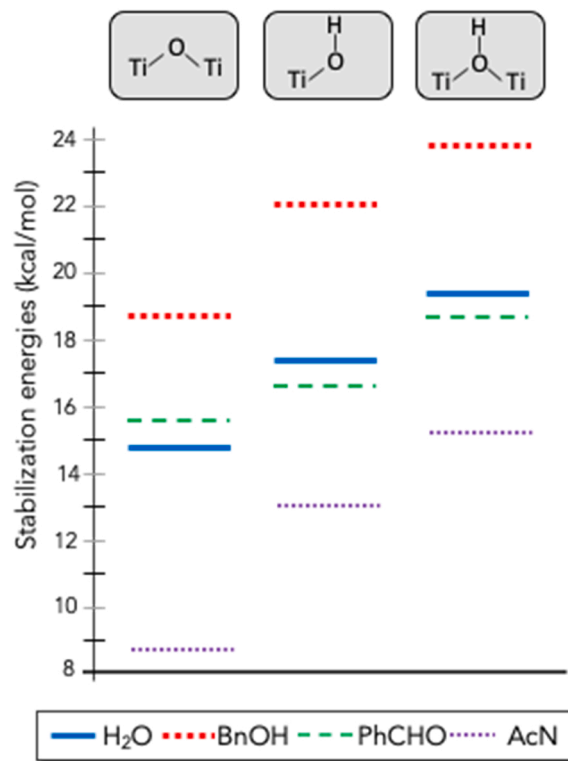

Fig. 7. Energies of adsorption of water, benzyl alcohol (BnOH), benzaldehyde (PhCHO) and acetonitrile (AcN) on different in nature surface functionalities (the exact values are presented in Table 2).

energies were obtained when hydrogen is attached to the bridging oxygen atom (hydrogenated oxygen bridging functionality). Benzyl alcohol presented the highest E_{Stab} and acetonitrile the lowest for all surface conformation. And maybe this is a critical reason that when the reaction takes place in water as solvent, the rate of BnOH conversion is dramatically lower comparing in acetonitrile as solvent due to the smaller difference in E_{Stab} [39]. Another worth to consider outcome is that hydrogen addition changes the stabilization energy difference between water and benzaldehyde. For tit, benzaldehyde is more stably adsorbed on the surface, but on the contrary, addition of a hydrogen reverses this trend. Additionally, the stabilization energy difference between benzaldehyde and acetonitrile is bigger for the non-hydrogen containing surface. The higher stability of water adsorption comparing to PhCHO as well as the lower of the stabilization energy difference between acetonitrile and PhCHO can explain why the home-made materials, that have a higher density of hydroxyl groups, have presented an elevated selectivity compared to P25.

From the point of view of the molecules' orientation upon adsorption/interaction with the surface (Fig. 8), benzyl alcohol has a skew orientation in the case of tit, while on tit-OH and tit-H its adsorbed parallelly to the surface, leading to a higher surface occupation comparing to skew and hence less molecules per surface can be adsorbed. It is important to point out that the alteration on the stabilization energy and orientation of the adsorbed BnOH on the surface alter the characteristic of the formed surface complex with a direct negative effect on the photosensitization/antenna effect in the case of the hydroxylated surfaces. In the case of benzaldehyde, a perpendicular to the surface orientation is favorable when adsorption occurs with tit and tit-H, while a parallel orientation is favorable upon adsorption through a hydroxyl group (tit-OH). Interestingly, in the case of tit and tit-H, BnOH has to change orientation upon oxidation to the corresponding aldehyde. Acetonitrile also showed a deviation in orientation of interaction, since it has preferably a parallel orientation for tit-OH and a skew to perpendicular for the other two surfaces.

3.5. Scavengers' tests

The utilization of scavengers to determine the ROSs responsible for the photoreactivity is a well know approach, although in various cases for the interpretation of the obtained results upon their utilizations, crucial factors are not considered in the literature. In general, two approaches can be followed for scavengers tests, the first one is to add the scavenger to a photocatalyst suspension without the targeted to be upgraded compound (in our case BnOH) and determine the formation of specific reactive species [48]. The second approach is to add the compound that will act as the scavenger in the reaction system in order to explore the direct effects during the photocatalytic reaction and to compare with the results without scavenger addition. Both approaches have positive and negative aspects, but in all cases some very crucial factors should always be considered.

In the case of organic scavengers, they can be also undergone photodecomposition or transformation, and hence their potential scavenging effect to dimmish by time. More importantly, the organic scavengers can interact with the targeted to be converted compound (or even by some products), forming complex moieties and hence to interfere the photocatalytic mechanism. Additionally, the compounds used as scavengers (or the compounds formed upon their photo-assisted transformation/decomposition) can be adsorbed or react (formation of complex) on specific sites on the photocatalyst's surface and either decreasing the catalytic activity or to led to alternative surface activation/reactivity. It is also plausible scavengers to act as light-scattering antennas upon interaction with the material's surface and so to influence the material's optical features [22]. Last but not lease, it should always be considered that the reactive species responsible for the first oxidation step, in our case of BnOH to PhCHO, can be responsible for the further oxidation/decomposition of the formed product upon oxidation
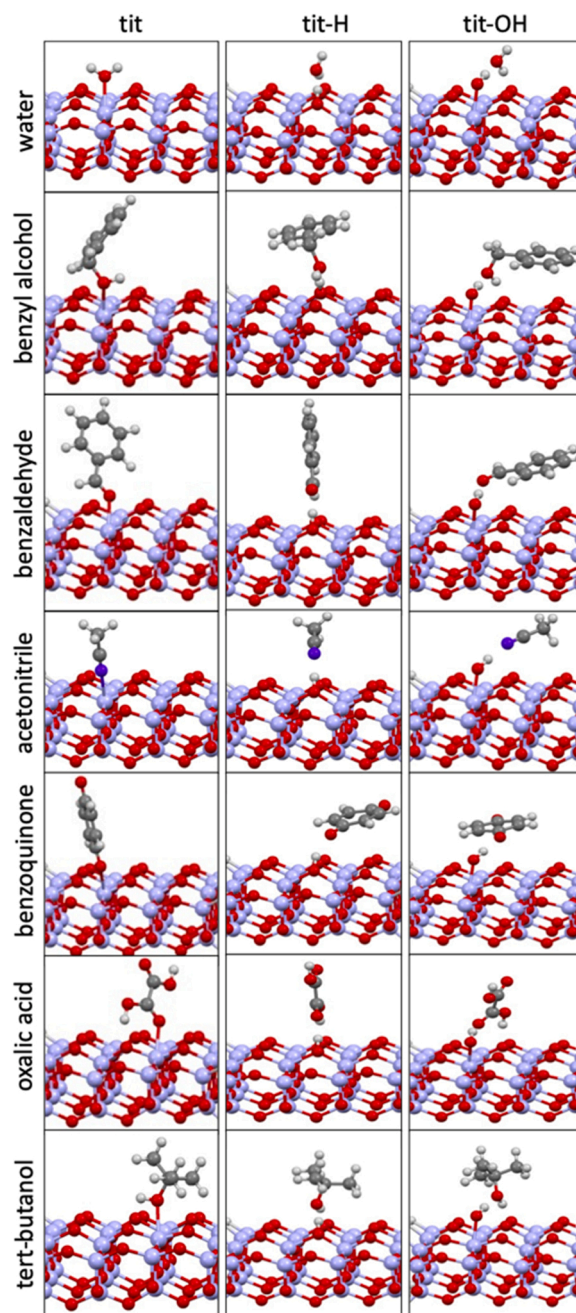

Fig. 8. The interaction of all the herein used organic compounds with a representative fragment of the titania surface as derived by DFT calculations.

of the initial compound. The presence of ionic scavenger can also lead to competitive phenomena upon their adsorption on specific sites on the material's surface blocking, like by affecting the adsorption extend, by altering the physicochemical features of the dispersion/suspension, or/and by forming surface complexes, and hence affecting the catalytic activity.

In order to investigate the involved ROSs in more details, different compounds, inorganic or organic, that can act as scavengers were used. Oxalic acid (OA) and potassium iodide (KI) were used as h^+ scavenger [21], silver nitrate (Ag) for e^- scavenger [22], 1,4-Benzoquinone (BQ) for $O_2^{\bullet-}$ scavenger [23], and tert-butanol (t-B) for $\bullet OH$ scavenger [21]. We used two holes scavengers since it is known that these photoinduced species play a determinantal role on benzyl alcohol photo-oxidation. It should also be pointed out that the amount of utilized compound as scavenger was in a one-to-one molar ratio to BnOH.

As discussed above, the targeted to be transformed compound can participate in a reaction with an active ROSs either being close to the surface where the active species are formed or by being pre-adsorbed on the catalyst's surface. Hence, the orientation and the strength of scavengers' adsorption can also play a decisive role that should be considered and so theoretical DFT calculations for the utilized organic scavengers were also performed with the results to be collected in Table 2 and Fig. 7. The observed trend for all molecules on the regards of energies of stabilization (E_{Stab}) is tit-H > tit-OH > tit. BQ showed the smaller stabilization energies comparing to OA and t-B, with the E_{Stab} to be in the range of acetonitrile but lower than BnOH, PhCHO, and water. OA showed E_{Stab} slightly higher than that of water. t-B showed the highest E_{Stab}, with values close to benzyl alcohol, a fact that brings in attention the possibility of competitive adsorption phenomena between BnOH and t-B, a fact that can have a negative impact on the adsorption/ oxidation rate. Regarding the orientation of interaction with the surface, OA has a perpendicular orientation, but in the case of tit with an angle. For BQ, the presence of hydrogen on the surface promotes the parallel orientation.

The intermolecular stabilization energies between all the organic compounds, interacting via hydrogen bonds in most cases, were also determined with the results presented in Table S1. Note that in some cases two different arrangements of the molecules were found. BnOH shows strong interaction with another BnOH molecule, as well as with BQ, t-B, and especially with OA. Acetonitrile showed significantly high energy of stabilization upon interaction by BnOH which is close for the interaction with another AcN molecule. Interestingly, AcN revealed the least value of stabilization energy for the interaction with PhCHO. PhCHO preferable interacts with water and BnOH, while the stabilization energy for interaction with AcN or PhCHO are low.

3.6. Mechanistic insight (scavengers tests) under Royal Blue irradiation

The results of benzyl alcohol oxidation evolution up to 6 h under RB light irradiation are collected in Fig. 9a, while for 24 h in Fig. 9b. The extension up to 24 h was chosen to additionally explore if the effect of scavenger can last and if so to which extend. In the case of P25, the addition of KI or OA (h^+ scavengers) led to an absolute diminishing of the photoreactivity. This is in a good correlation with the above discussed mechanisms, suggesting that holes are crucial for the initiation of the oxidation process. In the case of oxalic acid, a small extend of BnOH conversion occurred, linked to a partial photodecomposition of the organic acid (Fig. 9b). When an e^- scavenger (AgNO$_3$) was added, the BnOH conversion rate was not altered at the first 3 h for P25. Additionally, the formed PhCHO was further underwent unselective decomposition (no benzoic acid or other aromatic was detected), since the selectivity was less than 40% during the entire 6 h. After 24 h, the conversion was 25%, while the selectivity 27%. Scavenging of the photogenerated electrons had a positive impact on the e^-/h^+ separation, although in an extend in which the presence of holes led not only to the partial selective oxidation of benzaldehyde, but to other side reaction in which the formed PhCHO was further decomposed. The most important

observation is that both BnOH and PhCHO conversions were stopped after 3 h. Capturing of the generated e^- can prevent the e^-/h^+ recombination. Based on this, it would be expected that the addition of AgNO$_3$ will had a positive effect since the lifecycle of h^+ would be extended. On the contrary, the opposite occurred under RB irradiation, suggesting a different oxidation pathway in acetonitrile compared to an aqueous environment. In aqueous environment, holes can react with H$_2$O towards the formation of hydroxyl radicals, the species predominantly responsible for rational decomposition of PhCHO. It was previously reported that the addition of an electron scavenger led to increment of the BnOH photo-oxidation extent in water [23]. In our case, the presence of water is limited (pre-adsorbed humidity), and for that reason the photo-oxidation is stopped after 3 h, possible due to the transformation to OH radicals that were responsible for PhCHO decomposition. This can be further supported from the degradation of PhCHO only in the case of electron scavenger addition. Hence, the formation of the holes has a bifunctional role; to initiate the oxidation and to convert H$_2$O to free hydroxyl radicals. When the holes formation is limited, its participation is preferable towards initiation of the BnOH oxidation rather than to form •OH radicals, a fact that can be assigned also to the limited presence of pre-adsorbed water moieties. Additionally, scavenging of electrons obstruct the formation of superoxide anion radicals, and as a result the formation of •OOH and H$_2$O$_2$. Although, the formation of complex species that block the photocatalytic sites should not be excluded at this point.

Addition of •OH scavenger (t-B) increased slightly the conversion up to 6 h, a fact in a good correlation with the above described role of electrons and holes. The •OH presence is responsible for the further transformation of PhCHO as well as of poisoning the photoreactive sites. The formation of the •OH can be occurred through three pathways by the simultaneous consumption of dissolved O$_2$, H$_2$O or formed H$_2$O$_2$ (Fig. 4). Prolonging the reaction up to 24 h did not lead to further conversion, while the photodecomposition of PhCHO takes place with a negative impact of the PhCHO selectivity and yield, since tetr-butyl alcohol is consumed.

The most essential alteration was revealed upon BQ addition, since the conversion was dramatically increased for, reaching 67% after 3 h (~170% increment) and to 79% after 24 h. The increment of the photoreactivity had although and a negative effect on the yield since decomposition of PhCHO was also occurred. As reported by Zhao et. al [23], the addition of BQ when the reaction took place in aqueous environment, the formation of PhCHO was faster although the final amount was the same as without the addition of the scavenger, linking this effect to the involvement of O$_2^{\bullet-}$. Scavenging of species O$_2^{\bullet-}$ hinders the formation of "fresh" water and molecular oxygen via the decomposition of formed hydrogen peroxide, and subsequently the formation of hydroxyl radicals, since H$_2$O$_2$ is not formed.

To shed more light regarding the role of BQ, photolysis tests were also performed under RB as well as UV light irradiation with the results to be presented in Figures S7 and S8, respectively. While BnOH and PhCHO showed to be stable under RB irradiation, BQ was unstable, with a 93% of conversion to take place within 6 h. Interestingly, upon the co-presence of BQ and BnOH without catalyst, both organics revealed a similar trend of conversion, reaching a conversion of 68% and 63% for BnOH and BQ, respectively. This one-to-one conversion trend can suggest that these two compounds are form an intermediate complex which upon RB light exposure undergoes decomposition/oxidation. It is even more crucial to point out that the PhCHO yield after 6 h was 44%, suggesting that two third of BnOH undergo selective partial oxidation, while one third of the BnOH was decomposed to non-monoaromatic compound. The comparison with and without P25 revealed that the presence of catalyst elevated the BnOH conversion only slightly, both on the regards of the maximum conversion and its rate. Although and bearing in mind that P25 showed without BQ an almost 30% BnOH conversion, it would be expected that if the conversion of BnOH would be linked to both the photocatalytically activity of P25 and the presence

Table 2

The stabilization energies (in kcal/mol) of studied molecules with the model fragment of titania surface (cf. Fig. 8) and their orientation in relation to this surface.

	H$_2$O	BnOH	PhCHO	AcN	BQ	OA	t-B
	1.85	1.71	2.89	3.71	0.67		
tit	14.9	18.5	15.6	8.7	11.6	15.1	15.1
	n/a	/	∟	/∟	∟	/∟	n/a
tit-OH	17.7	22.0	16.5	13.2	14.2	18.0	19.7
	n/a	=	=	=	=	∟	n/a
tit-H	19.4	23.6	18.5	15.2	14.2	19.9	22.2
	n/a	=	∟	/∟	=	∟	n/a

∟ - perpendicular orientation, = parallel orientation, / - skew orientation.
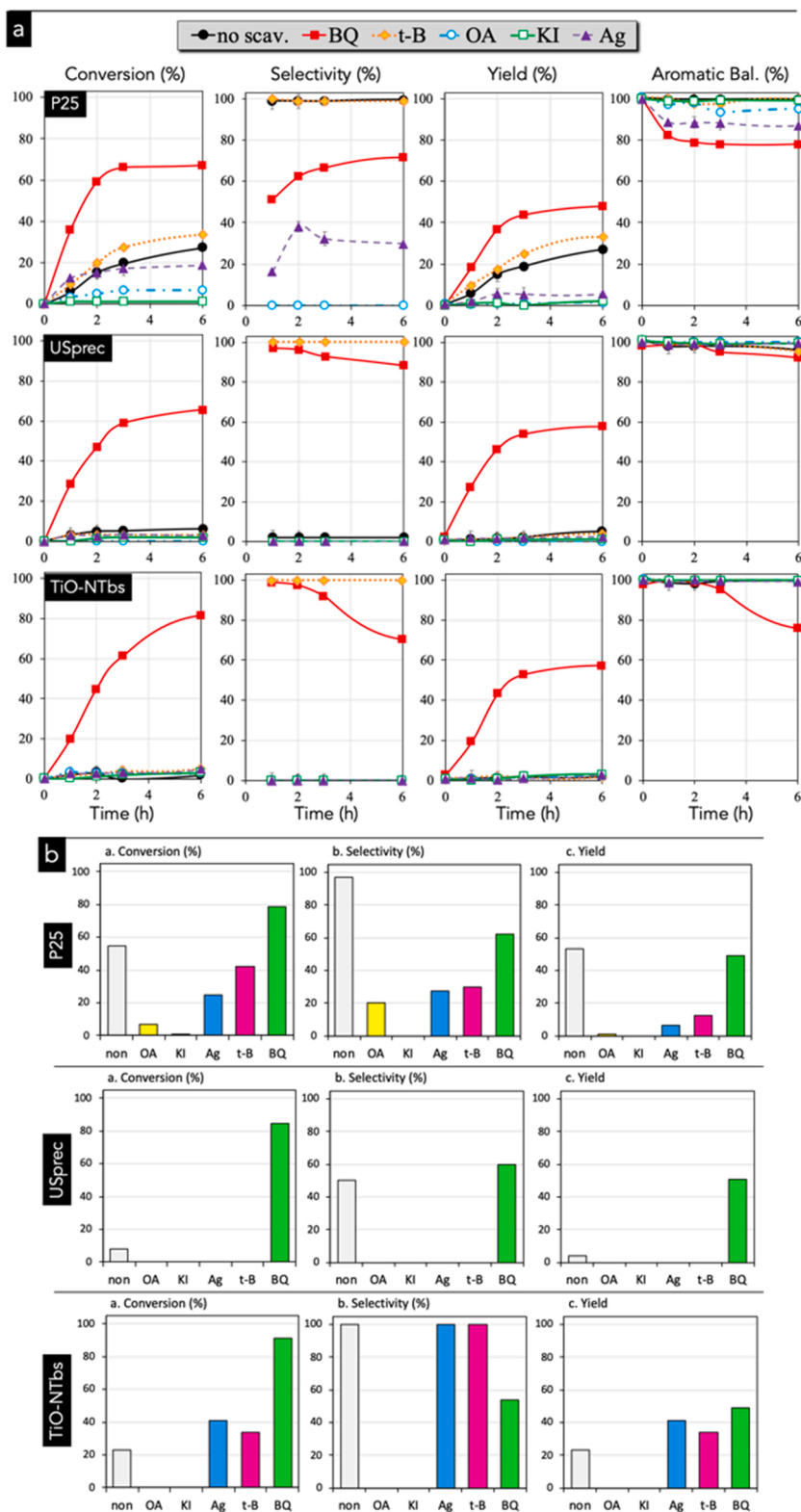
Fig. 9. Monitoring the BnOH conversion, PhCHO selectivity, PhCHP yield and aromatic balance (benzyl alcohol, benzaldehyde, benzoic acid) after the addition of various compounds used as scavengers (1,4-Benzoquinone (**BQ**), tert-butanol (**t-B**), oxalic acid (**OA**), potassium iodide (**KI**), and silver nitrate (**SN**)) for up to 6 h (a) and after 24 h (b) of royal blue (RB) light irradiation using TiO_2 P25, USprec, and TiO-NTbs.

of BQ, the final conversion would be around 90%. On the contrary and since the BnOH conversion was only ~65%, the presence of P25 showed that did not play a key role.

The positive impact of BQ addition was observed more intensively for USprec. This sample showed negligible photocatalytic efficiency to oxidize BnOH under RB light, while addition of BQ triggered the photo-assisted conversion. The BnOH conversion after 24 h reached 85% with the selectivity to be 60%, leading to the highest PhCHO yield under RB

irradiation (51%), the highest recorded for RB irradiation. The same trend of BnOH conversion activation was observed in the case of nanotubes (TiO-NTbs). The BnOH conversion was slightly higher (91%) comparing to USprec, although the lower selectivity (54%) led also to a lower PhCHO yield after 24 h (49%).

As above-mentioned, the home-made materials were inactive under RB irradiation. However, the addition of BQ initiated their photo-reactivity, with this effect to be slightly more pronounced for TiO-NTbs on the regards of BnOH conversion. This sample showed the highest amount of hydroxyl groups and more specifically the highest density of
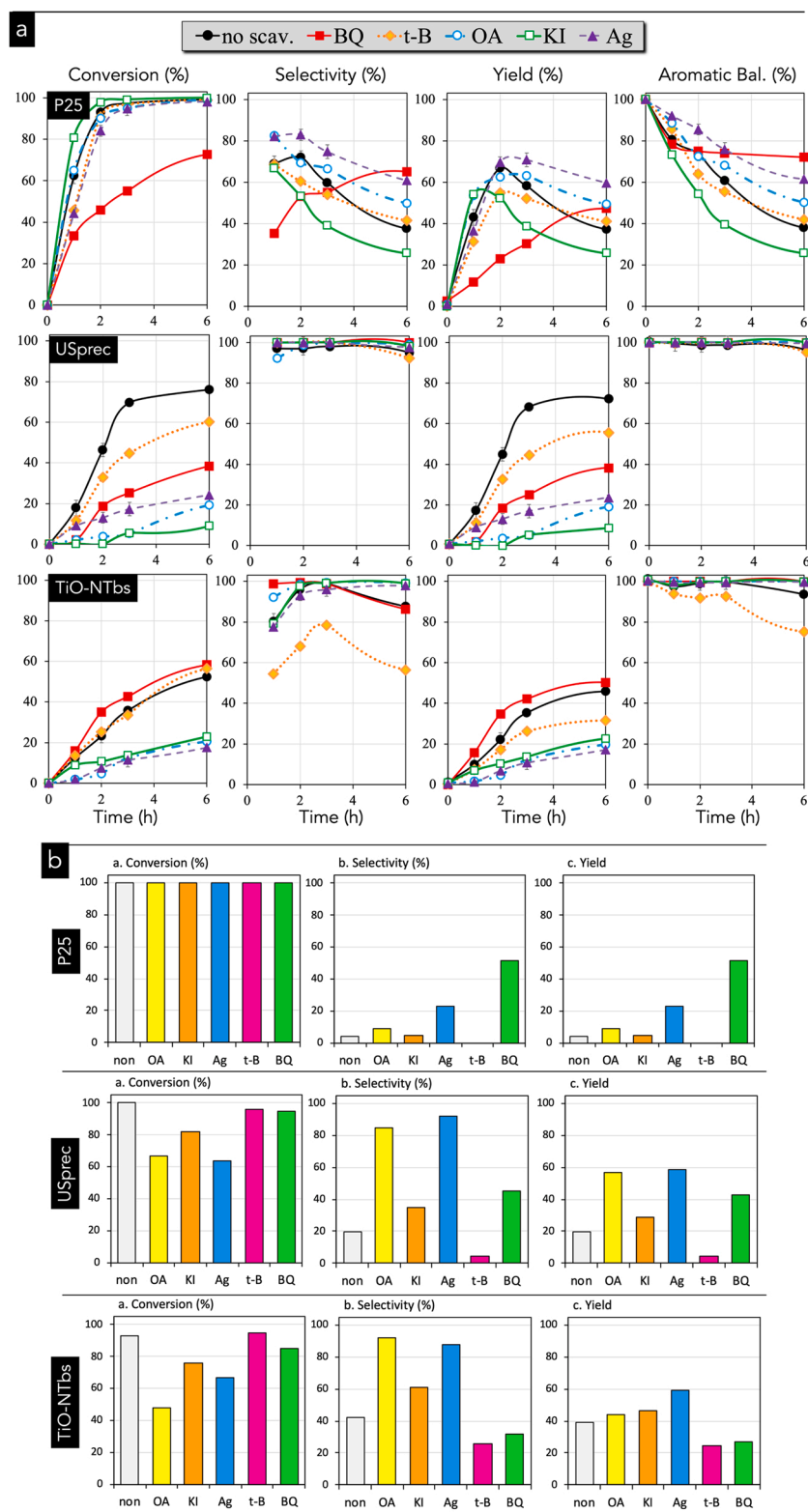
Fig. 10. Monitoring the BnOH % conversion, PhCHO % selectivity, PhCHP % yield and % aromatic balance (benzyl alcohol, benzaldehyde, benzoic acid) after the addition of various compounds used as scavengers (1,4-Benzoquinone (**BQ**), tert-butanol (**t-B**), oxalic acid (**OA**), potassium iodide (**KI**), and silver nitrate (**SN**)) for up to 6 h (a) and after 24 h (b) of ultraviolet (UV) light irradiation using TiO$_2$ P25, USprec, and TiO-NTbs.

surface functional groups with $pK_a > 7$ (linked to surface hydroxyl groups). So, it can be concluded (considering also the observed higher stabilization energy) that the interaction of BQ with the surface hydroxyl groups pronounced the photoreactive more intensively, comparing to Ti-O-Ti bridging groups. The main difference between USprec and TiO-NTbs upon BQ addition is that decomposition of the aromatic aldehyde took place more intensively for the titanate nanotubes, suggesting a different photooxidation mechanism. Hence, it can be concluded based on that the selectivity and yield of PhCHO upon BQ addition in the case of USprec and TiO-NTbs are higher in comparison to the photolysis tests, revealing a synergistic effect.

Another importance observation arisen by comparing the results of 24 h after addition of e⁻ and •OH scavengers between P25 and TiNTbs. For the former, the BnOH conversion was decreased, while for the latter increased. This different trend can be assigned to different oxidation mechanisms that are predominant for each material. Addition of e⁻ scavenger expect the better e^-/h^+ separation can lead to no O_2 consumption and the lower extend of $O_2^{\bullet-}$, H_2O_2, and •OH active species formation. Hence, it can be suggested that the predominant reaction pathway for P25 is the one showed in Fig. 5a. On the contrary, for TiNTbs addition of the e⁻ or •OH scavengers impact positively the BnOH conversion. This can suggest that the BnOH oxidation undergoes predominately thought the mechanism presented in Fig. 5c which can be further supported for the fact that the surface complex is favorite with the surface hydroxyl groups, as was also presented in previous studies [49].

In the herein presented and discussed results, no purging of O_2 or air was followed, hence the presence of molecular oxygen is due to the pre-existing dissolved amount. It should be mentioned that acetonitrile has a higher capacity for dissolved oxygen comparing to water [50–53]. The gradual rate decrement or/and termination of the BnOH to PhCHO oxidation can be explained also based on the O_2 consumption. The latter can be formed from the decomposition of H_2O_2, although, for its formation O_2 was consumed and the ratio of the consumed per formed is 2:1. In the case of the nanotubes, the presence of molecular oxygen is crucial towards the formation of the intermediate surface complex (Fig. 5c). When the tests were performed after sonication of the initial BnOH solution prior the addition of the catalyst in order to remove the dissolved oxygen (degassing) and by purging inert gas (nitrogen or argon) at the headspace of the reaction vessel, the conversion was almost eliminated under royal blue light irradiation.

3.7. Mechanistic insight (scavengers tests) under UV irradiation

As it was expected, a higher reactivity both on the regards of BnOH conversion and PhCHO decomposition was achieved for the three samples upon ultraviolet (UV) irradiation, with the results to be collected in Fig. 10. To interpret in detail the involved reactive species responsible for the photocatalytic activity in addition to determine precisely which mechanism is the predominant for each material were a complex and challenging process, especially bearing in mind that more than one reaction pathway was photocatalyzed. Although, analysis of the result under UV with the co-presence of various scavengers helped to extract specific conclusions. Additionally, we believe that this series of results and their discussion will trigger the attention and interest of the active in this field scientists to continue the research for the utilization of modified TiO_2-based semiconductor photocatalysts and to further explore the involved mechanism in each case.

Starting with TiO_2 P25, addition of KI resulted in increased BnOH conversion and PhCHO degradation rate, leading to the lowest aldehyde yield (26%) after 6 h. The scavenging of holes extends the lifetime of electrons, and so the formation of $O_2^{\bullet-}$ and H_2O_2 is pronounced, suggesting that upon UV irradiation these are essential active species for the selective partial oxidation of BnOH. $O_2^{\bullet-}$ and H_2O_2 are also responsible for the decomposition of PhCHO, since the selectivity was lower comparing without KI addition, and after 6 h the lowest value of yield

was observed. Interestingly, upon RB irradiation and KI addition, the same trend was observed for benzyl alcohol oxidation.

After the addition of OA or t-B, a similar trend as without the addition was observed, and this can be linked either to the negligible scavenging effect of OA or/and t-B or their (photo)decomposition. In the case of electron scavenging (Ag), even though the BnOH conversion rate was slightly decreased, a positive impact was observed for PhCHO selectivity, with the improvement to be around + 62% after 6 h comparing without a scavenger. This led to the highest PhCHO yield for P25 after 6 h (60%) and hence can be concluded that the elevated electron formation is not desirable from the perspective of PhCHO selectivity. The addition of BQ was escorted by markedly alteration in photoreactivity, since the BnOH conversion rate was intensively decreased to more than half for the first two hours. The photolysis tests of BQ under UV light showed a small decomposition the first 3 h (Figure S8). Considering the evolution of selectivity that had a continual incremental trend and the fact that the aromatic balance (benzyl alcohol, benzaldehyde and benzoic acid) was remained stable after 2 h, it can be concluded that initially the continual formed PhCHO was initially decompose for duration up to 1 h, but then its decomposition was of a significant lower extend. This suggests the unique role of $O_2^{\bullet-}$ both for the partial oxidation of BnOH as well as for the decomposition of PhCHO. Generally, for P25, the highest yield in the case of P25 was achieved between 2 and 3 h after addition of electrons scavenger, supporting that that h^+ and O_2 play the utmost essential role for BnOH selective partial oxidation. Analysis either by GC or HPLC did not reveal the formation either of other mono- or poly-aromatic compounds or of aliphatic compounds (with more that 4 carbons). Hence, the continuous decrement of the aromatic balance in linked to the unselective decomposition of BnOH and formed PhCHO to very small organic compounds or/and to mineralization to CO_2.

For the anatase core shell covered with amorphous porous phase nanoparticles (USprec) that showed without the addition of scavengers the highest PhCHO yield of 73% after 6 h of UV irradiation with an almost absolute selectivity (97%), the addition of any scavenger had a negative effect of BnOH conversion. The less negative impact was presented upon the addition of hydroxyl radical scavenger, followed by superoxide radical scavenger. Upon the addition of electrons or holes scavenger, the BnOH conversion rate was dramatically lower and even more interestingly in the case of h^+ scavenger addition, the initiation of the BnOH conversion occurred after 2 h. These results support our hypothesis that the photoreactivity of USprec is based on the formation of the surface complex and of various active oxygen containing species, with the hydroxyl radicals to have the least effect for both BnOH and PhCHO conversion.

Very remarkably for the titanate nanotubes, the co-presence of BQ did not affect its photocatalytic activity, suggesting that BnOH are preferably get adsorbed on the materials surface rather interactant with BQ molecules. Negligible was also the effect of OH radicals scavenger on BnOH conversion, although the selectivity was almost the half. This implies that the OH radicals have a multifunctional role, to consume electrons and as a result to promote the lifespan of photoinduced holes, except to be involved directly on the oxidation mechanism. Scavenging of e⁻ or h^+ led to a decrement of BnOH conversion rate almost by one third, confirming their determine function during photooxidation of BnOH and photo-assisted decomposition of PhCHO. It should be mentioned that when the degasification by sonication of the initial BnOH solution was performed prior the experiments and the inert gas was purged at the headspace of the reaction vessel during the entire photocatalytic tests, the BnOH conversion was significantly lower for all the materials, suggesting the important role of the dissolved molecular oxygen.

In Fig. 11 are collected the main conclusions derived from this work. We would like to conclude by pointing out that we evaluate under the same experimental conditions various know well-performing photocatalyst such as graphitic carbon nitride (g-C_3N_4) and its oxidized counterpart (gCNox) [54], composite of MOFs like HKUST-1 or UiO-66
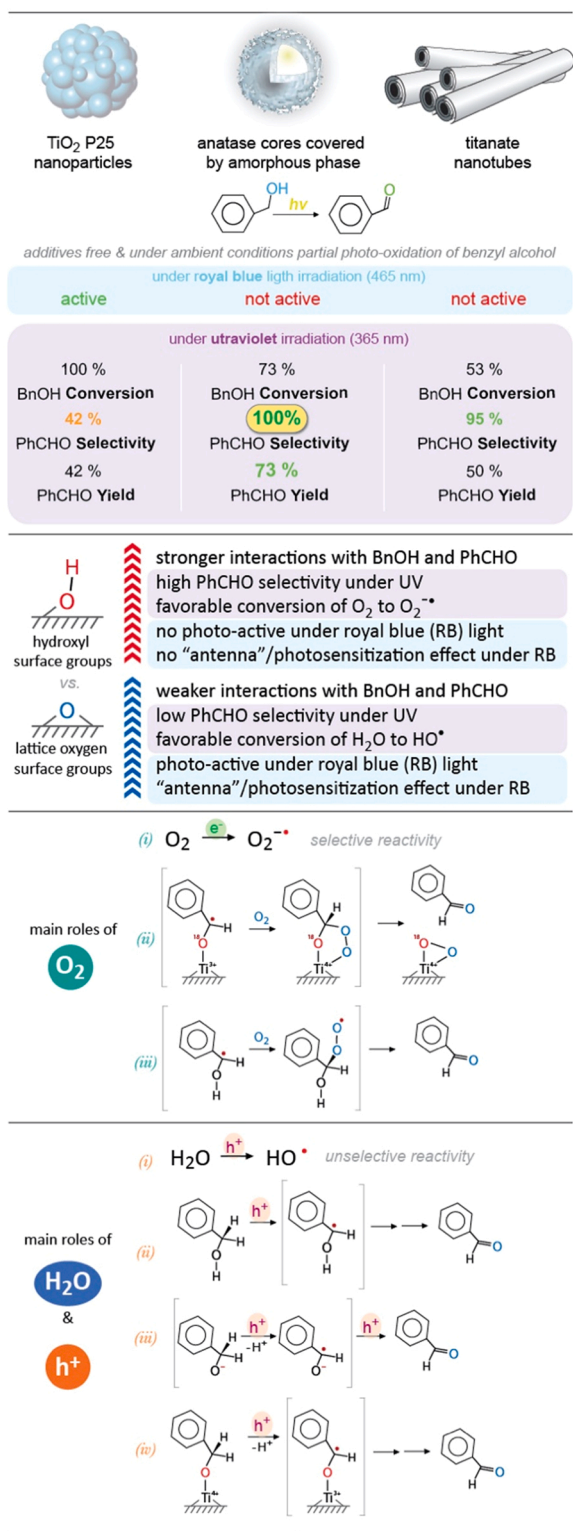
Fig. 11. The main key-conclusions upon the experimental and computational studies regarding the photocatalytic additive free partial oxidation of benzyl alcohol by titanium oxide/hydroxide based nanocatalyst under irradiation of low-power ultraviolet (365 nm) or royal-blue (465 nm) light at ambient conditions.

with graphite oxide or g-C$_3$N$_4$ [55–57], zinc oxide/hydroxide nano-materials [58]. Only g-C$_3$N$_4$ was found photoreactive but in significant lower extent than the three materials in which we focused in this work. A direct comparison with other materials presented in the literature was

out of the scope of this work, since the experimental conditions (temperature, pressure, amounts of catalyst per volume of initial BnOH solution, light intensity, reactor geometric parameters etc.) vary, establishing the comparison "tricky".

4. Conclusions

By monitoring the photocatalytic efficiency of various titanium oxide nano-photocatalysts for the additive-free selective partial oxidation of benzyl alcohol (BnOH) to the benzaldehyde (PhCHO) under ambient conditions and different in frequency light beam exposure (BnOH-2-PhCHO), we were able to determine and bring into the attention new and important insights for the involved mechanisms and the (reactive) species that are vital. Due to the variation of the nanocatalysts' textural, morphological, structural, as well as optical features and more importantly of the surface chemistry, essential outcomes were derived, in combination also with DFT calculations, regarding physicochemical features that play a key role.

The best performing nano-photocatalyst was the synthesized USprec nanoparticles (anatase core-shells covered with an amorphous porous phase rich in hydroxyl groups), that showed the highest PhCHO yield (73%) after 6 h of UV irradiation, with the selectivity to be almost 100%. Titanate nanotubes revealed also an acceptable BnOH conversion with a high PhCHO selectivity. The main general conclusion is that the photo-oxidation as well as the photo-decomposition of BnOH and of the derived compounds is a complicate and multi-mechanisms/reactions process when titanium (hydro)oxide based nanomaterials are used. Since no additives, like redox reagents, are used, the presence of pre-adsorbed water and pre-dissolved molecular oxygen is vital, as is presented by the "angel wings" photocatalytic cycles of the formation of all reactive oxygen-containing species (ROSs). Pre-adsorbed water is responsible for the formation of the hydroxyl radicals ($^{\bullet}$OH), as well as for blockage of catalytic sites. Dissolved molecular oxygen is involved at the formation of various ROSs, such as superoxide ($O_2^{-\bullet}$) and hydrogen superoxide ($\bullet$OOH) radicals. Dissolved O_2 is also involved in the formation of the "Ti side-on peroxide" from the BnOH-TiO$_2$ surface complex, while it can react also with a benzyloxy radical (PhCH$^{\bullet}$OH), with the product to transform finally to PhCHO.

The surface functional groups and especially the hydroxyl groups have a positive effect on the PhCHO selectivity, since they do not promote its further oxidation or decomposition. Based on DFT calculations, when the adsorption either of BnOH or PhCHO occurs via a terminal or bridging hydroxyl group, the complex is more stable and with a different orientation compared when the adsorption occurs by a lattice bridging oxygen. The orientation and the stronger adsorption "block" the photosensitization/antenna effect under royal blue light (465 nm) irradiation. In addition, in the case of hydroxylated titanium oxide surface, water is stronger adsorbed compared to benzaldehyde, and this is a reason for the latter not to further undergo photo-conversion. Scavenger tests revealed that the formation of two radicals plays a key role. On the one hand, the formation of the hydroxyl free radicals that are responsible for the unselective and uncontrolled oxidation and decomposition of both of BnOH and formed PhCHO. On the other hand, the radicals resulted from the molecular oxygen, and predominately the O$_2\bullet$-, are responsible for the partial oxidation of BnOH to PhCHO, without although to convert further the latter. The formation of holes is also important since they are involved in many photo-catalytic reactions. Another point of consideration upon scavengers' tests is that the results should be handled with care since various reactions can be responsible simultaneously for the photoreactivity and more importantly, side-effects and side-reactions can take place. As for instance was showed in this work, benzoquinone can potentially form dimer with BnOH that initiate their photolytic unselective conversion.

CRediT authorship contribution statement

Dimitrios A. Giannakoudakis: Writing – original draft, Writing – review & editing, Investigation, Conceptualization, Visualization. **Abdul Qayyum:** Investigation, Writing – original draft. **Mariusz Barczak:** Formal analysis (DFT calculations). **Ramón Fernando Colmenares-Quintero:** Writing – review & editing. **Piotr Borowski:** Formal analysis (DFT calculations). **Konstantinos Triantafyllidis:** Writing – review & editing, Conceptualization. **Juan Carlos Colmenares:** Writing – review & editing, Resources, Conceptualization, Project administration.

Declaration of Competing Interest

The authors declare that they have no known competing financial interests or personal relationships that could have appeared to influence the work reported in this paper.

Data availability

No data was used for the research described in the article.

Acknowledgments

Appendix A. Supporting information

Supplementary data associated with this article can be found in the online version at doi:10.1016/j.apcatb.2022.121939.

References

[1] C.-H. Zhou, X. Xia, C.-X. Lin, D.-S. Tong, J. Beltramini, Catalytic conversion of lignocellulosic biomass to fine chemicals and fuels, Chem. Soc. Rev. 40 (2011) 5588–5617, https://doi.org/10.1039/C1CS15124J.

[2] V. Nair, M.J. Muñoz-Batista, M. Fernández-García, R. Luque, J.C. Colmenares, Thermo-photocatalysis: environmental and energy applications, ChemSusChem 12 (2019) 2098–2116, https://doi.org/10.1002/cssc.201900175.

[3] M. Garedew, F. Lin, B. Song, T.M. DeWinter, J.E. Jackson, C.M. Saffron, C.H. Lam, P.T. Anastas, Greener routes to biomass waste valorization: lignin transformation through electrocatalysis for renewable chemicals and fuels production, ChemSusChem 13 (2020) 4214–4237, https://doi.org/10.1002/cssc.202000987.

[4] S.H. Li, S. Liu, J.C. Colmenares, Y.J. Xu, A sustainable approach for lignin valorization by heterogeneous photocatalysis, Green. Chem. 18 (2016) 594–607, https://doi.org/10.1039/c5gc02109j.

[5] S. Kumaravel, P. Thiruvengetam, K. Karthick, S.S. Sankar, A. Karmakar, S. Kundu, Green and sustainable route for oxidative depolymerization of lignin: New platform for fine chemicals and fuels, Biotechnol. Prog. 37 (2021), https://doi.org/10.1002/btpr.3111.

[6] P. Azadi, O.R. Inderwildi, R. Farnood, D.A. King, Liquid fuels, hydrogen and chemicals from lignin: A critical review, Renew. Sustain. Energy Rev. 21 (2013) 506–523, https://doi.org/10.1016/j.rser.2012.12.022.

[7] C. Xiao, L. Zhang, H. Hao, W. Wang, High Selective Oxidation of Benzyl Alcohol to Benzylaldehyde and Benzoic Acid with Surface Oxygen Vacancies on W18O49/Holey Ultrathin g-C3N4 Nanosheets, ACS Sustain. Chem. Eng. 7 (2019) 7268–7276, https://doi.org/10.1021/acssuschemeng.9b00299.

[8] C.M. Crombie, R.J. Lewis, R.L. Taylor, D.J. Morgan, T.E. Davies, A. Folli, D. M. Murphy, J.K. Edwards, J. Qi, H. Jiang, C.J. Kiely, X. Liu, M.S. Skjøth-Rasmussen, G.J. Hutchings, Enhanced Selective Oxidation of Benzyl Alcohol via in Situ H2O2Production over Supported Pd-Based Catalysts, ACS Catal. 11 (2021) 2701–2714, https://doi.org/10.1021/acscatal.0c04586.

[9] X. Bao, H. Li, Z. Wang, F. Tong, M. Liu, Z. Zheng, P. Wang, H. Cheng, Y. Liu, Y. Dai, Y. Fan, Z. Li, B. Huang, TiO2/Ti3C2 as an efficient photocatalyst for selective oxidation of benzyl alcohol to benzaldehyde, Appl. Catal. B: Environ. 286 (2021) 119885, https://doi.org/10.1016/j.apcatb.2021.119885.

[10] M.J. Lima, A.M.T. Silva, C.G. Silva, J.L. Faria, N.M. Reis, Selective photocatalytic synthesis of benzaldehyde in microcapillaries with immobilized carbon nitride, Chem. Eng. J. 430 (2022), https://doi.org/10.1016/j.cej.2021.132643.

[11] A. Akhundi, A. Badiei, G.M. Ziarani, A. Habibi-Yangjeh, M.J. Muñoz-Batista, R. Luque, Graphitic carbon nitride-based photocatalysts: Toward efficient organic transformation for value-added chemicals production, Mol. Catal. 488 (2020), 110902, https://doi.org/10.1016/j.mcat.2020.110902.

[12] D.S.M. Constantino, M.M. Dias, A.M.T. Silva, J.L. Faria, C.G. Silva, Intensification strategies for improving the performance of photocatalytic processes: A review, J. Clean. Prod. 340 (2022), https://doi.org/10.1016/j.jclepro.2022.130800.

[13] A.V. Vorontsov, P.G. Smirniotis. Environmentally Benign Photocatalysts: Applications of Titanium Oxide-based Materials, 1st ed.,, Springer,, New York, New York, 2010, https://doi.org/10.1007/978-0-387-48444-0.

[14] C. Berberidou, G.Z. Kyzas, I. Paspaltsis, T. Sklaviadis, I. Poulios, Photocatalytic disinfection and purification of water employing reduced graphene oxide/TiO2 composites, J. Chem. Technol. Biotechnol. 94 (2019) 3905–3914, https://doi.org/10.1002/jctb.6188.

[15] S. Peiris, H.B. de Silva, K.N. Ranasinghe, S.V. Bandara, I.R. Perera, Recent development and future prospects of TiO2 photocatalysis, J. Chin. Chem. Soc. 68 (2021) 738–769, https://doi.org/10.1002/jccs.202000465.

[16] M.J. Lima, M.J. Sampaio, C.G. Silva, A.M.T. Silva, J.L. Faria, Magnetically recoverable Fe 3 O 4 /g-C 3 N 4 composite for photocatalytic production of benzaldehyde under UV-LED radiation, Catal. Today 328 (2019) 293–299, https://doi.org/10.1016/j.cattod.2018.11.018.

[17] J.F.J.R. Pesqueira, M.F.R. Pereira, A.M.T. Silva, A life cycle assessment of solar-based treatments (H2O2, TiO2 photocatalysis, circumneutral photo-Fenton) for the removal of organic micropollutants, Sci. Total Environ. 761 (2021), https://doi.org/10.1016/j.scitotenv.2020.143258.

[18] D.A. Giannakoudakis, N. Farahmand, D. Łomot, K. Sobczak, T.J. Bandosz, J. C. Colmenares, Ultrasound-activated TiO2/GO-based bifunctional photoreactive adsorbents for detoxification of chemical warfare agent surrogate vapors, Chem. Eng. J. 395 (2020) 125099, https://doi.org/10.1016/j.cej.2020.125099.

[19] D.A. Giannakoudakis, A. Qayyum, D. Łomot, M.O. Besenhard, D. Lisovytskiy, T. J. Bandosz, J.C. Colmenares, Boosting the Photoactivity of Grafted Titania: Ultrasound-Driven Synthesis of a Multi-Phase Heterogeneous Nano-Architected Photocatalyst, Adv. Funct. Mater. 31 (2021) 1–7, https://doi.org/10.1002/adfm.202007115.

[20] D.A. Giannakoudakis, K. Vikrant, A.P. LaGrow, D. Lisovytskiy, K.-H. Kim, T. J. Bandosz, J. Carlos Colmenares, Scrolled titanate nanosheet composites with reduced graphite oxide for photocatalytic and adsorptive removal of toxic vapors, Chem. Eng. J. 415 (2021), 128907, https://doi.org/10.1016/j.cej.2021.128907.

[21] Y. Chen, S. Yang, K. Wang, L. Lou, Role of primary active species and TiO2 surface characteristic in UV-illuminated photodegradation of Acid Orange 7, J. Photochem. Photobiol. A: Chem. 172 (2005) 47–54, https://doi.org/10.1016/j.jphotochem.2004.11.006.

[22] S. Higashimoto, N. Suetsugu, M. Azuma, H. Ohue, Y. Sakata, Efficient and selective oxidation of benzylic alcohol by O2 into corresponding aldehydes on a TiO2 photocatalyst under visible light irradiation: Effect of phenyl-ring substitution on the photocatalytic activity, J. Catal. 274 (2010) 76–83, https://doi.org/10.1016/j.jcat.2010.06.006.

[23] L. Zhao, B. Zhang, X. Xiao, F.L. Gu, R.Q. Zhang, Roles of the active species involved in the photocatalytic oxidation of benzyl alcohol into benzaldehyde on TiO2 under UV light: Experimental and DFT studies, J. Mol. Catal. A: Chem. 420 (2016) 82–87, https://doi.org/10.1016/j.molcata.2016.03.012.

[24] X. Li, J.L. Shi, H. Hao, X. Lang, Visible light-induced selective oxidation of alcohols with air by dye-sensitized TiO2 photocatalysis, Appl. Catal. B: Environ. 232 (2018) 260–267, https://doi.org/10.1016/j.apcatb.2018.03.043.

[25] C.J. Li, G.R. Xu, B. Zhang, J.R. Gong, High selectivity in visible-light-driven partial photocatalytic oxidation of benzyl alcohol into benzaldehyde over single-crystalline rutile TiO 2 nanorods, Appl. Catal. B: Environ. 115–116 (2012) 201–208, https://doi.org/10.1016/j.apcatb.2011.12.003.

[26] R. Li, H. Kobayashi, J. Guo, J. Fan, Visible-light induced high-yielding benzyl alcohol-to-benzaldehyde transformation over mesoporous crystalline TiO2: A self-adjustable photo-oxidation system with controllable hole-generation, J. Phys. Chem. C. 115 (2011) 23408–23416, https://doi.org/10.1021/jp207259u.

[27] C.Y. Wang, R. Pagel, J.K. Dohrmann, D.W. Bahnemann, Antenna mechanism and de-aggregation concept: Novel mechanistic principles for photocatalysis, Mater. Sci. Forum 544– 545 (2007) 17–22, https://doi.org/10.1016/j.crci.2005.02.053.

[28] S. Higashimoto, N. Kitao, N. Yoshida, T. Sakura, M. Azuma, H. Ohue, Y. Sakata, Selective photocatalytic oxidation of benzyl alcohol and its derivatives into corresponding aldehydes by molecular oxygen on titanium dioxide under visible light irradiation, J. Catal. 266 (2009) 279–285, https://doi.org/10.1016/j.jcat.2009.06.018.

[29] A. Magdziarz, J.C. Colmenares, O. Chernyayeva, D. Lisovytskiy, J. Grzonka, K. Kurzydłowski, K. Freindl, J. Korecki, Insight into the synthesis procedure of Fe3+/TiO2-based photocatalyst applied in the selective photo-oxidation of benzyl alcohol under sun-imitating lamp, Ultrason. Sonochem. 38 (2017) 187–196, https://doi.org/10.1016/j.ultsonch.2017.03.012.

[30] C.-Y. Wu, K.-J. Tu, J.-P. Deng, Y.-S. Lo, C.-H. Wu, Markedly Enhanced Surface Hydroxyl Groups of TiO2 Nanoparticles with Superior Water-Dispersibility for Photocatalysis, Materials 10 (2017) 566, https://doi.org/10.3390/ma10050566.

[31] A. Khan, M. Goepel, A. Kubas, D. Łomot, W. Lisowski, D. Lisovytskiy, A. Nowicka, J.C. Colmenares, R. Gläser, Selective oxidation of 5-hydroxymethylfurfural to 2,5-diformylfuran by visible light-driven photocatalysis over in situ substrate-sensitized titania, ChemSusChem 14 (2021) 1351–1362, https://doi.org/10.1002/cssc.202002687.

[32] H. Kobayashi, S. Higashimoto, DFT study on the reaction mechanisms behind the catalytic oxidation of benzyl alcohol into benzaldehyde by O2 over anatase TiO2 surfaces with hydroxyl groups: role of visible-light irradiation, Appl. Catal. B: Environ. 170– 171 (2015) 135–143, https://doi.org/10.1016/j.apcatb.2015.01.035.

[33] X. Yan, Y. Li, T. Xia, Black titanium dioxide nanomaterials in photocatalysis, Int. J. Photo 2017 (2017), https://doi.org/10.1155/2017/8529851.

[34] A. Naldoni, M. Altomare, G. Zoppellaro, N. Liu, Š. Kment, R. Zbořil, P. Schmuki, Photocatalysis with reduced TiO 2: From Black TiO 2 to cocatalyst-free hydrogen production, ACS Catal. 9 (2019) 345–364, https://doi.org/10.1021/acscatal.8b04068.

[35] B. Ohtani, O.O. Prieto-Mahaney, D. Li, R. Abe, What is Degussa (Evonic) P25? Crystalline composition analysis, reconstruction from isolated pure particles and photocatalytic activity test, J. Photochem. Photobiol. A: Chem. 216 (2010) 179–182, https://doi.org/10.1016/j.jphotochem.2010.07.024.

[36] F. Parrino, M. Bellardita, E.I. García-López, G. Marcì, V. Loddo, L. Palmisano, Heterogeneous photocatalysis for selective formation of high-value-added molecules: some chemical and engineering aspects, ACS Catal. 8 (2018) 11191–11225, https://doi.org/10.1021/acscatal.8b03093.

[37] V. Augugliaro, T. Caronna, V. Loddo, G. Marcì, G. Palmisano, L. Palmisano, S. Yurdakal, Oxidation of aromatic alcohols in irradiated aqueous suspensions of commercial and home-prepared rutile TiO2: A selectivity study, Chem. - A Eur. J. 14 (2008) 4640–4646, https://doi.org/10.1002/chem.200702044.

[38] A.K. Datye, G. Riegel, J.R. Bolton, M. Huang, M.R. Prairie, Microstructural characterization of a fumed titanium dioxide photocatalyst, J. Solid State Chem. 115 (1995) 236–239, https://doi.org/10.1006/jssc.1995.1126.

[39] D.A. Giannakoudakis, D. Łomot, J.C. Colmenares, When sonochemistry meets heterogeneous photocatalysis: designing a sonophotoreactor towards sustainable selective oxidation, Green. Chem. 22 (2020) 4896–4905, https://doi.org/10.1039/D0GC00329H.

[40] I. Velo-Gala, A. Torres-Pinto, C.G. Silva, B. Ohtani, A.M.T. Silva, J.L. Faria, Graphitic carbon nitride photocatalysis: The hydroperoxyl radical role revealed by kinetic modelling, Catal. Sci. Technol. 11 (2021) 7712–7726, https://doi.org/10.1039/d1cy01657a.

[41] E. Kusmierek, A CeO2, semiconductor as a photocatalytic and photoelectrocatalytic material for the remediation of pollutants in industrial wastewater: A review, Catalysts 10 (2020) 1–54, https://doi.org/10.3390/catal10121435.

[42] C. Zheng, G. He, X. Xiao, M. Lu, H. Zhong, X. Zuo, J. Nan, Selective photocatalytic oxidation of benzyl alcohol into benzaldehyde with high selectivity and conversion ratio over Bi4O5Br2 nanoflakes under blue LED irradiation, Appl. Catal. B: Environ. 205 (2017) 201–210, https://doi.org/10.1016/j.apcatb.2016.12.026.

[43] G. Palmisano, G. Scandura, V. Augugliaro, V. Loddo, A. Pace, B.S. Tek, S. Yurdakal, L. Palmisano, Unexpectedly ambivalent O2 role in the autocatalytic photooxidation of 2-methoxybenzyl alcohol in water, J. Mol. Catal. A: Chem. 403 (2015) 37–42, https://doi.org/10.1016/j.molcata.2015.03.021.

[44] M.J. Pavan, H. Fridman, G. Segalovich, A.I. Shames, N.G. Lemcoff, T. Mokari, Photoxidation of Benzyl Alcohol with Heterogeneous Photocatalysts in the UV Range: The Complex Interplay with the Autoxidative Reaction, ChemCatChem 10 (2018) 2541–2545, https://doi.org/10.1002/cctc.201800284.

[45] X. Xiao, C. Zheng, M. Lu, L. Zhang, F. Liu, X. Zuo, J. Nan, Deficient Bi24O31Br10as a highly efficient photocatalyst for selective oxidation of benzyl alcohol into benzaldehyde under blue LED irradiation, Appl. Catal. B: Environ. 228 (2018) 142–151, https://doi.org/10.1016/j.apcatb.2018.01.076.

[46] S. Higashimoto, N. Suetsugu, M. Azuma, H. Ohue, Y. Sakata, Efficient and selective oxidation of benzylic alcohol by O2into corresponding aldehydes on a TiO2photocatalyst under visible light irradiation: Effect of phenyl-ring substitution on the photocatalytic activity, J. Catal. 274 (2010) 76–83, https://doi.org/10.1016/j.jcat.2010.06.006.

[47] X.F. Zhang, Z. Wang, Y. Zhong, J. Qiu, X. Zhang, Y. Gao, X. Gu, J. Yao, TiO 2 nanorods loaded with Au–Pt alloy nanoparticles for the photocatalytic oxidation of benzyl alcohol, J. Phys. Chem. Solids 126 (2019) 27–32, https://doi.org/10.1016/j.jpcs.2018.10.026.

[48] D.A. Giannakoudakis, M. Florent, R. Wallace, J. Secor, C. Karwacki, T.J. Bandosz, Zinc peroxide nanoparticles: Surface, chemical and optical properties and the effect of thermal treatment on the detoxification of mustard gas, Appl. Catal. B: Environ. 226 (2018) 429–440, https://doi.org/10.1016/j.apcatb.2017.12.068.

[49] A. Khan, M. Goepel, W. Lisowski, D. Łomot, D. Lisovytskiy, M. Mazurkiewicz-Pawlicka, R. Gläser, J.C. Colmenares, Titania/chitosan-lignin nanocomposite as an efficient photocatalyst for the selective oxidation of benzyl alcohol under UV and visible light, RSC Adv. 11 (2021) 34996–35010, https://doi.org/10.1039/d1ra06500a.

[50] J.M. Achord, C.L. Hussey, Determination of dissolved oxygen in nonaqueous electrochemical solvents, Anal. Chem. 52 (1980) 601–602, https://doi.org/10.1021/ac50053a061.

[51] D.A. Giannakoudakis, V. Nair, A. Khan, E.A. Deliyanni, J.C. Colmenares, K. S. Triantafyllidis, Additive-free photo-assisted selective partial oxidation at ambient conditions of 5-hydroxymethylfurfural by manganese (IV) oxide nanorods, Appl. Catal. B: Environ. 256 (2019), 117803, https://doi.org/10.1016/j.apcatb.2019.117803.

[52] F. Vendruscolo, M.J. Rossi, W. Schmidell, J.L. Ninow, Determination of Oxygen Solubility in Liquid Media, ISRN Chem. Eng. 2012 (2012) 1–5, https://doi.org/10.5402/2012/601458.

[53] Q. Li, C. Batchelor-Mcauley, N.S. Lawrence, R.S. Hartshorne, R.G. Compton, Anomalous solubility of oxygen in acetonitrile/water mixture containing tetra-n-butylammonium perchlorate supporting electrolyte; The solubility and diffusion coefficient of oxygen in anhydrous acetonitrile and aqueous mixtures, J. Electroanal. Chem. 688 (2013) 328–335, https://doi.org/10.1016/j.jelechem.2012.07.039.

[54] D.A. Giannakoudakis, M. Seredych, E. Rodríguez-Castellón, T.J. Bandosz, Mesoporous graphitic carbon nitride-based nanospheres as visible-light active chemical warfare agents decontaminant, ChemNanoMat 2 (2016) 268–272, https://doi.org/10.1002/cnma.201600030.

[55] D.A. Giannakoudakis, T.J. Bandosz, Building MOF nanocomposites with oxidized graphitic carbon nitride nanospheres: the effect of framework geometry on the structural heterogeneity, Molecules 24 (2019) 4529, https://doi.org/10.3390/molecules24244529.

[56] D.A. Giannakoudakis, N.A. Travlou, J. Secor, T.J. Bandosz, Oxidized g-C 3 N 4 Nanospheres as Catalytically Photoactive Linkers in MOF/g-C 3 N 4 Composite of Hierarchical Pore Structure, Small 13 (2017), 1601758, https://doi.org/10.1002/smll.201601758.

[57] D.A. Giannakoudakis, T.J. Bandosz, Defectous UiO-66 MOF Nanocomposites as Reactive Media of Superior Protection against Toxic Vapors, ACS Appl. Mater. Interfaces 12 (2020) 14678–14689, https://doi.org/10.1021/acsami.9b17314.

[58] D.A. Giannakoudakis, J.A. Arcibar-Orozco, T.J. Bandosz, Key role of terminal hydroxyl groups and visible light in the reactive adsorption/catalytic conversion of mustard gas surrogate on zinc (hydr)oxides, Appl. Catal. B: Environ. 174 (2015) 96–104, https://doi.org/10.1016/j.apcatb.2015.02.028.